Mathematical billiards: Periodic orbits within quadrilaterals

Hongjia H. Chen
The University of Auckland

Abstract

Mathematical billiards is a dynamical system that models billiards in an idealised environment. The billiard ball is considered to be a point mass and satisfies the law of reflection when interacting with the boundary; the shape of the mathematical billiard is arbitrary. These simple constraints lead to surprisingly deep and complex dynamics. We focus on billiards with quadrilateral boundaries. The existence of periodic orbits in all polygons is currently one of the most resistant problems in dynamics. This dissertation makes progress on this conjecture and explores the existence of periodic orbits within squares, rectangles and parallelograms. We provide alternative proofs to classical results for square billiards with additional insights and connections to number theory. We also take a dynamical systems approach which enables the use of bifurcation theory and parameter continuation. We introduce a novel continuation formulation which bypasses the extreme degeneracies exhibited by mathematical billiards and use it to compute branches of periodic solutions as a parameter varies the shape of the billiard from a square to a rectangle and parallelogram. The insights gained from the numerical exploration lead us to prove that there exist no period-4 orbits within the parallelogram and to show in a computer-assisted manner the existence of a bifurcation diagram that exhibits a period-adding sequence, where a periodic orbit has its period change under parameter variation in successive jumps of four each time.

Contents

Chapter 1

Introduction

Mathematical billiards shares many similarities to the game of billiards (pool) in reality. Fundamentally, both comprise of a billiard ball that bounces off the sides of a table. In reality, the table is almost always a rectangle, but mathematical billiards can be played on tables of arbitrary shapes and dimensions. Mathematical billiards ignore friction, takes the billiard as a point mass and assumes elastic collisions. As a consequence, the billiard trajectory will satisfy the law of reflection (*the angle of incidence equals the angle of reflection*) when it bounces off a boundary. Due to these constraints, mathematical billiards is readily applied to optics. First posed as Alhazen's problem [2] by Ptolemy in 150 AD, mathematical billiards has had a plethora of applications including but not limited to the computation of π [17], quantum computing [16] and mechanics [7, 32, 37, 38], pouring problems [29], Benford's Law [34], diffusion in Lorentz Gas [13] and the Riemann hypothesis [6].

Definition 1.1. A billiard table $\mathcal{D} \subset \mathbb{R}^2$ is an open bounded connected domain with boundary $\partial\mathcal{D}$.

We define the tuples (α_i, P_i) where α_i is the anti-clockwise angle between $\partial\mathcal{D}$ and the trajectory after collision, P_i is the position of the collision on $\partial\mathcal{D}$. The billiard map F determines the next angle and position according to the law of reflection.

Definition 1.2. For a map F, a set of points $(\alpha_0, P_0), (\alpha_1, P_1), ..., (\alpha_{n-1}, P_{n-1})$ with $(\alpha_i, P_i) = F(\alpha_{i-1}, P_{i-1})$ for $i = 1, ..., n$ is a periodic orbit (of least period n) if $F(\alpha_{n-1}, P_{n-1}) = (\alpha_0, P_0)$ and $(\alpha_{i+k}, P_{i+k}) \neq (\alpha_i, P_i)$ for any k with $0 < k < n$.

In billiard theory, periodic orbits are of great interest and importance. For quadrilaterals, each side is a line such that $\alpha_i \in (0, \pi)$, it is then sufficient to consider trajectories with $\alpha_0 \in (0, \frac{\pi}{2}]$, because for a periodic orbit, the initial angle $\pi - \alpha_0$ yields a trajectory in the opposite direction (time-reversal symmetry). The existing literature on periodic orbits within billiards is separated into two categories, namely, smooth and non-smooth billiard tables $\mathcal{D}$. If $\mathcal{D}$ is a smooth convex body, such as the circle and ellipse, then it typically exhibits more predictable and non-chaotic behaviour such that phase portraits can be used to examine invariant curves in phase space, periodic orbits and chaotic regions [18]. The regions are separated by caustics, these are curves along which a billiard trajectory is tangent [30]. If $\mathcal{D}$ is non-smooth, its point(s) of zero curvature are vertices or cusp points. The presence of these points result in chaotic dynamics where a perturbation in the initial condition will drastically change the long-term behaviour of the trajectory. Furthermore, such $\mathcal{D}$ do not have any caustics and periodic orbits comprise of measure 0 in phase space [25].

Mathematical billiard has extensively been studied from the perspective of algebraic geometry (moduli spaces), Teichmüller and ergodic theory with three textbooks published [10, 30, 34]. However there remains a myriad of unsolved open problems in billiards [14, 19]. Perhaps the most well known are problem 3 of Katok's five most resistant problems in dynamics [21] and the Triangular Billiards Conjecture [31]:

Open Problem 1. Is there a periodic orbit for any polygonal $\mathcal{D} \subset \mathbb{R}^2$?

Open Problem 2. Every trianglular $\mathcal{D}$ has a periodic orbit.

It is clear why Open Problem 1 is one of the most difficult problems in dynamics as the triangular billiard conjecture is a special case that is itself a 200-year old conjecture [31]. In general, it is known that periodic trajectories are dense in polygons with angles that are rational multiples of π [5]. We find through a literature review and correspondence with authors of billiard textbooks and researchers that there is very little known regarding parallelogram billiards. The non-existence of odd periodic orbits has been proven for parallelograms with angle $\frac{\pi}{3}$ radians (two equilateral triangles glued together) [1]. Also the non-existence of stable periodic orbits which persist under perturbations do not exist for parallelograms with angle $\frac{\pi}{4}$ radians [30]. We take a different approach using ideas from dynamical systems to study billiards which extend more readily to these open problems.

The dissertation is set up as follows. In chapter 2 we provide an overview on the theory for square billiards, we also provide alternative proofs, new insights including a connection to number theory and extend the results to the rectangular billiard. In chapter 3, we present a dynamical systems approach to the billiard problem. We demonstrate that this representation satisfies the theoretical results from chapter 2 and discuss the degeneracy of billiards that leads to a singular parameter continuation problem. Chapter 4 proposes a novel formulation that addresses the degeneracy problems. We follow periodic orbits from the square to both the rectangle and the parallelogram. We present new and surprising results on the existence of periodic orbits and bifurcations within the parallelogram. Finally computer code, numeric results and proofs of lemmas can be found in the Appendix.

Chapter 2

Square Billiards

The square billiard is the simplest non-smooth billiard table, but the results are often briefly skimmed over. It is introduced early on in billiard textbooks, typically alongside the circular billiard [10, 30, 34]. The vertices of the square provide distinct behaviour from the circular and convex tables, they are readily analysed by the powerful technique of unfolding.

We consider trajectories within the unit-square $\mathcal{D} = \{(x, y)|\ 0 < x < 1, 0 < y < 1\}$ as the geometry of the trajectory is invariant under the rescaling of the square. For brevity, label each of the vertices A, B, C and D in anti-clockwise manner as depicted in Figure 2.1. We identify the boundary of the square with the interval $[0, 4)$ such that the sub-intervals $[0, 1), [1, 2), [2, 3), [3, 4)$ represents sides AB, BC, CD, DA, respectively. Thus $P \in [0, 4)$ and $\alpha \in (0, \pi)$. At the four vertices, the tangent line for reflection is not defined. We stipulate that the trajectory terminates if the trajectory collides with the vertex. Interesting and important dynamics occur when trajectories narrowly avoid the vertices [5].

Consider the following introductory examples of trajectories in the square. It is sufficient to consider trajectories that initially leave side AB as the labelling of vertices is arbitrary. When the trajectory leaves the boundary at an angle of $\alpha = \frac{\pi}{2}$, we have a period-2 orbit as illustrated in Figure 2.1(a). If the billiard leaves with $\alpha = \frac{\pi}{4}$, we will have a period-4 orbit as shown in Figure 2.1(b). Note that for panels (a) and (b), the angles remain constant throughout the trajectory. In Figure 2.1(c), we have a period-6 orbit with $\alpha = \text{atan}(2)$ and $P = 0.2$. We show later that the periodicity of almost all trajectories is uniquely defined by the initial angle; initial positions that result in alternative behaviour are a set of measure 0. The square billiard has the special and rare property that it is *ergodically optimal* [12]:

Definition 2.1. A billiard table is ergodically optimal if for all trajectories that avoid the vertices, one of the following holds: the trajectory is either periodic or uniformly dense.

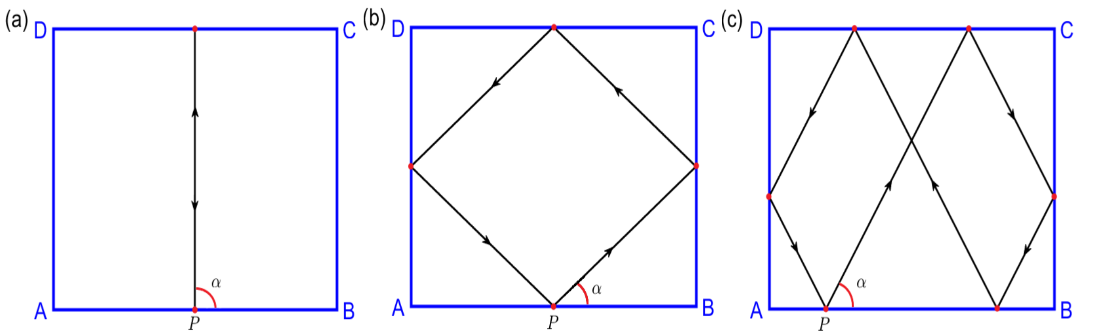

Figure 2.1: Examples of periodic orbits in the square billiard. Panels (a) with $(\alpha, P) = (\frac{\pi}{2}, 0.5)$, (b) with $(\alpha, P) = (\frac{\pi}{4}, 0.5)$ and (c) with $(\alpha, P) = (\text{atan}(2), 0.2)$ show examples of period-2, period-4 and period-6 orbits, respectively.

2.1 Unfolding billiards

Following the billiard trajectory inside a square billiard $\mathcal{D}$ can be difficult due to the myriad of self-intersections. Suppose that, instead of the trajectory reflecting off the boundary, the table itself reflects, so that the trajectory remains a straight line. For every collision between the billiard and the boundary, we reflect the table based on the side of the collision. Figure 2.2 illustrates this for the first five reflections of an arbitrary initial condition. The trajectory is shown in $\mathcal{D}$ in panel (a) and in a series of successively reflected tables in panel (b). We denote unfolded representation as $\mathbb{R}^2_S$. Horizontal reflections of $\mathcal{D}$ correspond to the trajectory colliding with the adjacent sides (BC & AD) relative to the initial orientation of $\mathcal{D}$. Vertical reflections correspond to the billiard colliding with the opposite sides (AB & CD). The unfolding process is invertible, we can obtain the original trajectory in $\mathcal{D}$ by folding the tiling back together.

Notice that in Figure 2.2(b) that the orientation of the square changes each time a collision occurs. More precisely, there are four unique orientations of squares in $\mathbb{R}^2_S$; see already in Figure 2.3(a). We define a coordinate system on $\mathbb{R}^2_S$ with orientation. The initial/original square table is located at vertices $\{(0,0),(0,1),(1,0),(1,1)\}$ and has positive orientation both in horizontal and vertical directions. The reflected tables are then defined by the integer coordinate vertices in $\mathbb{R}^2_S$ with the following orientations:

Definition 2.2. For a tiled square with bottom-left vertex $(x, y) \in \mathbb{R}^2_S$,

- if x is even then the square has positive horizontal orientation
- if x is odd then the square has negative horizontal orientation
- if y is even then the square has positive vertical orientation
- if y is odd then the square has negative vertical orientation

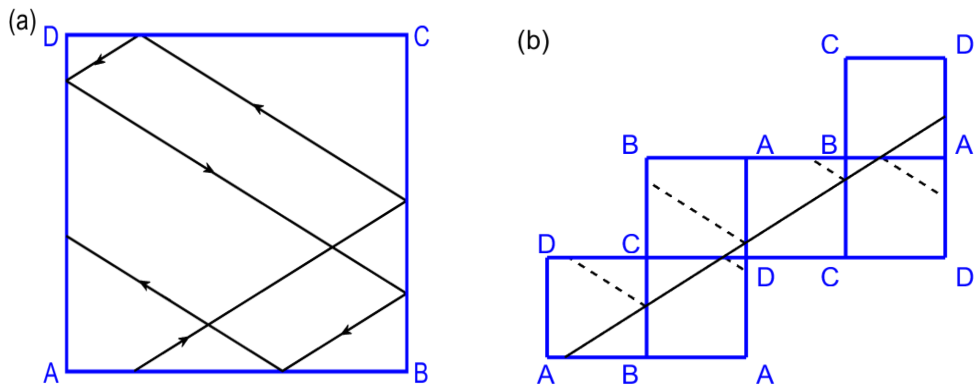

Figure 2.2: A trajectory within the square billiard and the associated unfolding. Panel (a) illustrates five reflections of a trajectory starting from side AB. Panel (b) shows the corresponding trajectory unfolded with five table reflections. Dotted black lines indicate the trajectory based on the law of reflection.

2.2 Classical proof for periodicity conditions

From the unfolding process described in Section 2.1, there are four unique orientations. It suffices to analyse the trajectory using the 2×2 square grid given by the four squares within $\{(x, y)|\ 0 \leq x \leq 2, 0 \leq y \leq 2\}$, which we denote by $\mathbb{K}_S$. Figure 2.3(a) depicts $\mathbb{K}_S$ with an arbitrary trajectory and illustrate how trajectories disappear off the edge of the squares. Borrowing verbatim from Strogatz [33]: "the trajectory reappears on the opposite side." The trajectory is given by several parallel lines, which is reminiscent of the flow on a torus. We can equivalently represent our square as a torus by gluing the top and bottom edges together to form a cylinder and then gluing the ends of the cylinder together as shown in Figure 2.3(b). We then use the following fundamental result from differential geometry regarding geodesics on a torus [28]:

Theorem 2.3. *If the slope of the line in the square is rational/(irrational), then there is a closed geodesic on the torus/(the closure is the entire torus).*

The theorem readily extends to periodic orbits in the square billiard:

Corollary 2.4. *If the trajectory within the square billiard is periodic, then the slope is rational.*

Since we only require that the slope tan(α) is rational, the periodicity within the square billiard appears to depend only on the initial angle and not the initial position. It is not immediately clear with this argument that a rational slope is only a necessary condition for periodicity in the

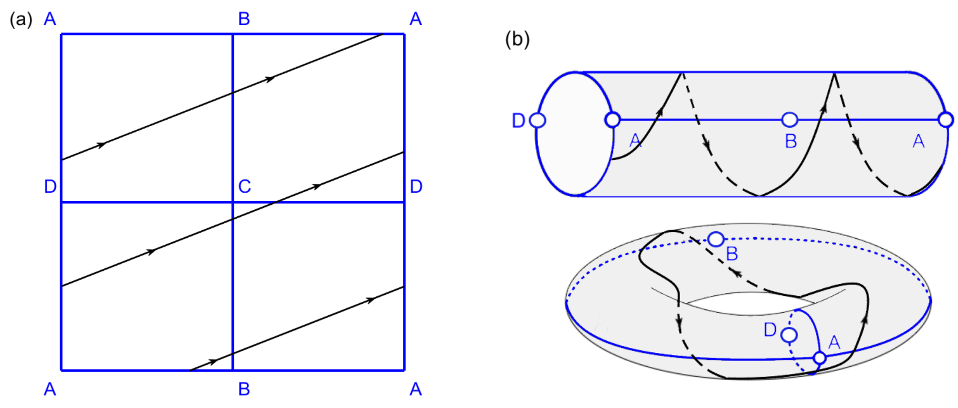

Figure 2.3: Equivalent representations of a trajectory in the square billiard. Panel (a) illustrates the trajectory on $\mathbb{K}_S$ with the four unique square orientations. In panel (b), the top and bottom sides of $\mathbb{K}_S$ are identified to form a cylinder and, subsequently, the adjacent sides are identified to form a torus.

square, because it does not account for the trajectories that end in a vertex. Trajectories with irrational slopes (that avoid vertices) are uniformly dense[1] [10, 34]. Hence, the square billiard table is ergodically optimal.

This is the standard proof given in billiard textbooks. The result is brief due to the advanced mathematical concepts used. However the brevity sacrifices important properties within the square billiard such as the non-existence of odd periodic orbits [11] and it is unclear what the period of the billiard trajectory will be for a given rational slope.

2.3 Odd periods within the square billiard

In this section, we provide an alternative and more intuitive proof that reproduces the necessary condition for periodicity and also provides the additional insight addressed earlier.

Proposition 2.5. *There do not exist period-3 trajectories within the square billiard.*

Proof. Suppose for the sake of contradiction that a period-3 trajectory exists. The period-3 trajectory must collide with the square boundary at exactly 3 unique points which we denote as P, Q and R. Hence, the trajectory forms a triangle PQR inscribed within the square ABCD. Each of these points must reside on a unique side of the square as it is impossible for the billiard to

[1]Remark: Textbook by Rozikov [30, Remark 3.1] states: “the trajectory is dense. This happens when the angle at which we shoot the ball is an irrational multiple of π.” This statement is incorrect.

collide twice in a row with the same side. We illustrate such a possible period-3 orbit in Figure 2.4; we denote the angles at which the trajectory leaves each side as α, θ and β; note that the trajectory in Figure 2.4 is not a true solution due to error in reflection at R. The remaining angles follow from the law of reflection. From triangle PBQ, we find that $\theta = \frac{\pi}{2} - \alpha$, and from triangle QCR, we have $\beta = \alpha$. Furthermore, $\alpha = \pi - \beta$ due to the quadrilateral APRD. Therefore, we must have $\alpha = \frac{\pi}{2}$, but then the trajectory is a period-2 trajectory that only collides with the boundary at two unique points, P and R; a contradiction. $\square$

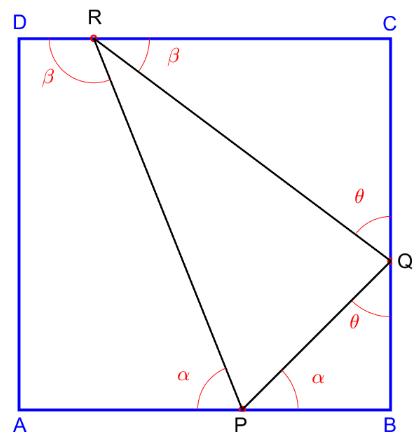

Figure 2.4: Candidate period-3 orbit within the square ABCD. The triangle PQR describes the trajectory and the angles α, θ and β are given by the law of reflection.

We cannot easily extend this geometric proof for other odd periods as the billiard trajectory self-intersects for larger periods. This motivates the use of the unfolding technique introduced in Section 2.1 which is immune to the self-intersection problem.

Instead of restricting ourselves to $\mathbb{K}_S$ used in the classical proof, we allow the unfolding to continue indefinitely on $\mathbb{R}^2_S$. If we denote the initial angle as $\alpha \in (0, \frac{\pi}{2}]$, the slope of the trajectory is $\tan(\alpha)$. It suffices to consider only $\alpha \in (0, \frac{\pi}{2}]$ as periodic trajectories with initial angles in the interval $(\frac{\pi}{2}, \pi)$, i.e., $\pi - \alpha$, only differ in the direction of the billiard. Since we have time reversal symmetry, we assume $\alpha \in (0, \frac{\pi}{2}]$ in the sequel.

Theorem 2.6. *If a billiard trajectory is periodic in the square then the slope of the trajectory is rational. Furthermore, all periodic trajectories of the square have even period.*

Proof. Consider a trajectory starting with (α, P) where P is a distance of x_0 away from vertex A. In $\mathbb{R}^2_S$, a periodic orbit requires the trajectory to return back to a side AB at distance x_0

away from A. Suppose it takes p vertical reflections of the table and q horizontal reflections, for some p, $q \in \mathbb{N}$, before we return back to the initial position. The period is then $p+q$ and the slope of the trajectory $\tan(\alpha) = \frac{p}{q} \in \mathbb{Q}$ can be determined by using the dashed triangle in Figure 2.5. Furthermore, the trajectory must intersect P again with positive vertical and horizontal orientation as otherwise once we fold the tiling, the trajectory will be travelling in the opposite direction (angle $\pi - \alpha$). By Definition 2.2, this occurs when we have undergone an even number of vertical reflections and an even number of horizontal reflections. Thus, $p = 2m$ and $q = 2n$ for some $m, n \in \mathbb{N}$, and the period is $2(m+n)$. Hence, for trajectories of the square to be periodic, the slope must be rational and the subsequent period is even. □

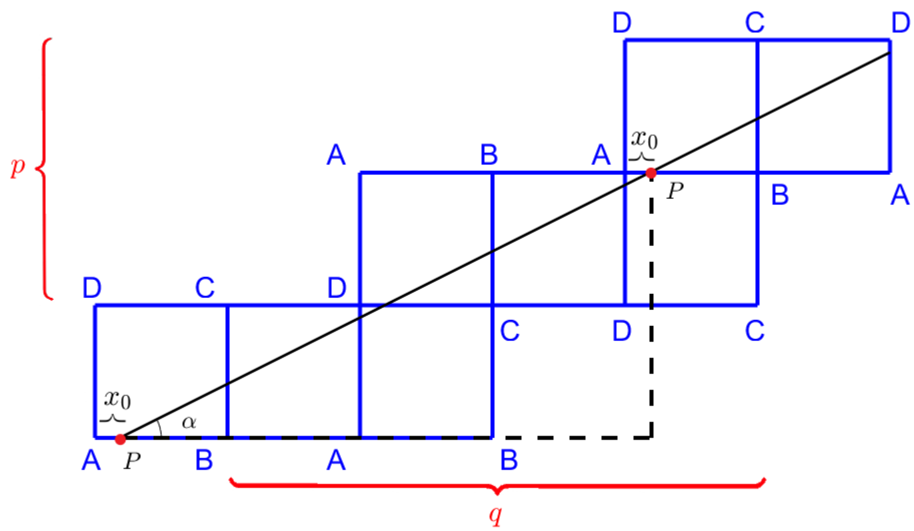

Figure 2.5: Candidate trajectory in $\mathbb{R}^2_S$ with p vertical and q horizontal reflections before returning to the initial position P.

We see that periodicity on $\mathbb{R}^2_S$ is determined almost entirely by the initial angle. However, particular initial positions with rational slopes also result in non-periodic trajectories. The rational slope is a necessary condition, but not sufficient. Trajectories with rational slopes can end up in the vertices and thus are non-periodic and singular. These initial conditions are referred to as pre-images of the vertices and are discussed in Section 2.4. The advantage of the classical proof for periodicity in Section 2.3 is that it is more easily extended to higher dimensions than the proof for Theorem 2.6. Inside the n-dimensional hypercube billiard, the motion of the trajectory is reduced to rotation on the torus $\mathbb{T}^{n-1}$ [34].

If the trajectory is periodic, then the unfolded trajectory will intersect P on side AB infinitely many times. The least period is when the trajectory *first* intersects P, or equivalently, the least number of collisions with the boundary before arriving back to the initial position and angle. Consider the periodic orbit generated with an initial angle atan$(\frac{p}{q})$ where $\frac{p}{q} \in \mathbb{Z}$. Setting $\alpha = \text{atan}\left(\frac{dp}{dq}\right)$ for any $d \neq 0$ gives rise to an identical periodic orbit. Then the period $p + q$ is *least* if for all $d \in \{3, ..., \min\{p, q\}\}$, $\frac{p}{d} \notin \mathbb{N}$ and $\frac{q}{d} \notin \mathbb{N}$, which motivates the following definition[2].

Definition 2.7. Given a periodic trajectory with p vertical reflections and q horizontal reflections. The period $p + q$ is the *least* period of the trajectory if gcd$(p, q) = 2$.

Since the number of vertical and horizontal reflections is even, $p = 2m$ and $q = 2n$ for some $m, n \in \mathbb{N}$. If $p + q$ is the least period, then gcd$(p, q) = 2$ which implies gcd$(n, m) = 1$. Therefore n and m are co-prime. As a result of this, for any given initial angle/slope, simplify the fraction $\tan(\alpha)$ until the numerator and denominator are co-prime (irreducible). The least period is twice the sum of the co-prime numerator and denominator. For example, to generate a period-4 trajectory such as in Figure 2.1(b), we find $n, m \in \mathbb{N}$ such that $2(n+m) = 4$ which also satisfies gcd$(n, m) = 1$. The only such candidate is $n = m = 1$. Therefore, the initial angle will be $\alpha = \text{atan}(1) = \frac{\pi}{4}$.

To generate a billiard trajectory with least period T, we can take $n = 1$ and $m = \frac{T}{2} - 1$, or vice versa, which is guaranteed to satisfy Definition 2.7. However, this is the trivial decomposition, there are typically other decompositions of $\frac{T}{2}$ into the sum of two co-prime numbers available. To find the number of possible decompositions, we use Euler's totient function from number theory [24]. For any $N \in \mathbb{N}$, Euler's totient function $\varphi(N)$ counts the number of natural numbers $k \in \{1, \dots, N\}$ such that gcd$(k, N) = 1$. The integers k that satisfy this property are referred to as *totatives* of N. Note that the number of pairs[3] $(m, n) \in \mathbb{N} \times \mathbb{N}$, with gcd$(m, n) = 1$ and $N = m + n$ is equal to $\varphi(N)$; a proof can be found in Section A.1 located in the Appendix. For $T = 2N$, there are $\varphi(N)$ unique angles in the interval $(0, \frac{\pi}{2}]$ which produce a period-T trajectory within the square billiard.

The classical technique to compute Euler's totient function is Euler's product formula, $\varphi(N) = N \prod\limits_{p|N} \left(1 - \frac{1}{p}\right)$ where the product is over the distinct prime factors of N. As an example, consider periodic trajectories with period $T = 10$. The number of possible decompositions is $\varphi(N) = 4$, which are (up to order): $T = 2(4 + 1)$ and $T = 2(3 + 2)$; hence, there are four different period-10 orbits with one, two, three and four points on the side AB of the square billiard.

[2] A similar definition for the equilateral triangle is given in [3]

[3] Remark: This is sequence A225530 in OEIS.

2.4 Vertex pre-images within the square billiard

In this section, we analyse singular trajectories in the square billiard. The initial conditions that result in a singular trajectory are denoted as pre-images of the vertices; these are also referred to as generalised diagonals in the literature [5]. Pre-images exist for both rational and irrational slopes. The natural method of finding pre-images is to start at a vertex with varying initial angles[4], then the pre-images end up in the vertex by time reversal. Furthermore, there are pre-images of different orders as some initial conditions may require many collisions before ending up in a vertex and some require very few. In Figure 2.6(a) we depict a period-6 orbit that narrowly avoids vertices A and B, Figure 2.6(b) displays a trajectory with the same initial angle that collides with the vertices; we conclude that $(\alpha_0, P_0) = (\text{atan}(2), 0.5)$ leads to a singular trajectory after one collision. Figure 2.6(c) shows a trajectory initialised at vertex A with $\alpha_0 = \text{atan}(\frac{3}{2})$ and terminates at B after three collisions. Consider a trajectory starting from a vertex, we define the order of pre-images as the total number of billiard reflections until we terminate at another vertex. We can find the order of pre-images by examining the trajectory in $\mathbb{R}^2_S$. In Figure 2.7, we have trajectories starting from vertex A with slopes of 4, $\frac{2}{3}$ and $\frac{5}{4}$ which each have pre-images of order three, three and seven, respectively.

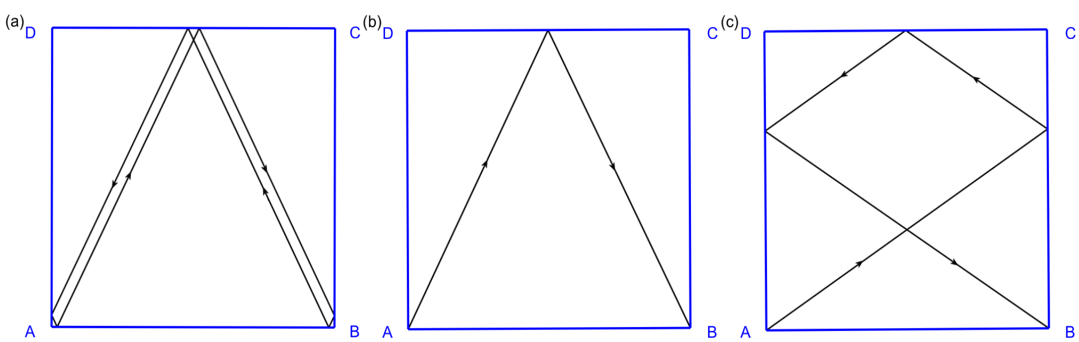

Figure 2.6: Examples of pre-images of vertices within the square. Panel (a) depicts a period-6 orbit that narrowly avoids vertex A and B. Panel (b) shows the pre-image of vertices A and B for the initial angle atan(2). Panel (c) depicts a trajectory starting from vertex A with angle atan$\left(\frac{3}{2}\right)$ which reflects three times before terminating in vertex B.

Proposition 2.8. *If a trajectory starts at a vertex with an irrational slope, then the trajectory never collides with another vertex in the square billiard.*

Proof. Suppose for the sake of contradiction that an irrational slope does result in the trajectory encountering another vertex. Using its representation in $\mathbb{R}^2_S$, say the trajectory starts at $(0, 0)$

[4] We can initialize at a vertex as the billiard does not reflect from its initial position.

and passes through the point (q, p). By Definition 2.2, the locations of the vertices must be in $\mathbb{Z} \times \mathbb{Z}$. Hence the slope of the line is then $\frac{p}{q} \in \mathbb{Z}$ and is rational; a contradiction. $\square$

Corollary 2.9. *If a billiard trajectory starts at a vertex with a rational slope, then the trajectory will always end up in a vertex in the square billiard.*

With an irrational slope, the order of pre-images is infinite, because Proposition 2.8 implies that we do not terminate at a vertex, and by Theorem 2.6, the trajectory is not periodic. On the other hand, with a rational slope the order of pre-images is finite, because the trajectory terminates at another vertex. The order of pre-images is well defined and depends only on the period of the trajectory (not the slope itself) that the rational slope typically yields.

Proposition 2.10. *For a trajectory in the square billiard that starts at a vertex with a slope that yields period-T orbits when the initial position is not a pre-image of the vertex. Then the order of pre-images is given by $\frac{T}{2} - 2$.*

Proof. Consider a trajectory starting from $(0, 0) \in \mathbb{R}^2_S$. Let $m, n \in \mathbb{N}$ such that $\gcd(m, n) = 1$ and set the slope as $\frac{m}{n}$. By Theorem 2.6 and Definition 2.7, this gives a least period-T orbit where $T = 2(m + n)$ if we do not start from a pre-image of the vertex. By Proposition 2.8, the trajectory intersects the point (m, n) which is a vertex. From $(0, 0)$ to (m, n), we have $m - 1$ horizontal reflections and $n - 1$ vertical reflections. Thus from $(0, 0)$, the trajectory collides with with the boundary of the square billiard $m + n - 2$ times before terminating in (m, n). Hence, the pre-image will be of order $\frac{T}{2} - 2$. $\square$

For example, the slopes $\frac{4}{1}, \frac{3}{2}, \frac{2}{3}, \frac{1}{4}$ all yield three pre-images as these slopes produce period-10 trajectories within the square; see the green and magenta lines in Figure 2.7. Combining Proposition 2.10 with Corollary A.2, there are $\varphi(\frac{T}{2})$ angles that produce period-T trajectories and all these angles, when initialised at a vertex, yield pre-images of order $\frac{T}{2} - 2$.

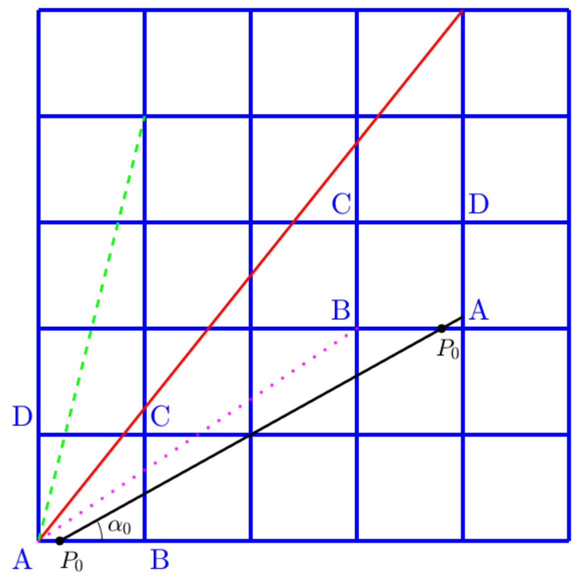

Figure 2.7: Pre-images of the vertex A determined via forward trajectories from A on $\mathbb{R}^2_S$. The trajectories in solid red, dashed green and dotted magenta are given by slopes of $\frac{5}{4}$, 4 and $\frac{2}{3}$, respectively. The solid black trajectory depicts a $\mathbb{R}^2_S$ representation of a trajectory that visits (α_0, P_0) and $(\pi - \alpha_0, P_0)$ in the square.

Proposition 2.11. [5] *If a trajectory passes through a point P in the square billiard, with angle $\alpha \neq \frac{\pi}{2}$, then it cannot return to P with angle $\pi - \alpha$.*

Proof. Suppose that there exits a trajectory starting with (α_0, P_0) on side AB and for some $k \in \mathbb{N}$, $(\alpha_k, P_k) = (\pi - \alpha_0, P_0)$ in $\mathcal{D}$. We give a candidate trajectory that intersects (α_0, P_0) and (α_k, P_k) in the $\mathbb{R}^2_S$ representation in Figure 2.7 (solid black line). An angle of $\pi - \alpha_0$ corresponds to the trajectory travelling from side AB to AD which requires a square with positive vertical and negative horizontal orientation. By Definition 2.2, the bottom-left vertex has odd x-coordinate and even y-coordinate. It is more convenient to work with the bottom-right vertex which then must have even x and y-coordinates which we denote as $(2n, 2m)$, where $n, m \in \mathbb{N}$. In $\mathbb{R}^2_S$, the trajectory intersects the points $(P_0, 0)$ and $(2n - 2x_0, 2m)$ which gives the rise to the line: $\{(x, y) \in \mathbb{R}^2_S | y = \frac{m}{n - x_0}(x - x_0)\}$. But at the midpoint of this trajectory, where $x = n$, we will have $y = m$. Thus, the trajectory intersects (n, m), which is a vertex, before reaching $(2n - 2x_0, 2m)$. Therefore, the trajectory encounters a vertex before reaching $(\pi - \alpha_0, P_0)$. $\square$

[5] The proposition is reminiscent of illumination problems [34, 35].

2.5 Rectangular billiards

The natural and most straightforward extension from the square is to the rectangle. The rectangular boundary most accurately models a billiard table in reality where the aspect ratio of side lengths is $2:1$. Consider a rectangle with side lengths a and b, where $b \leq a$. The aspect ratio of the rectangle is the ratio of the greater side length versus the lesser side length (a square has aspect ratio $1:1$). The unfolded tiling for the rectangle is denoted as $\mathbb{R}^2_R$ and is related to $\mathbb{R}^2_S$ by the linear transform: $(x, y) \to (ax, by)$. A sample unfolding with a period-6 orbit is given in Figure 2.8.

Proposition 2.12. *If a trajectory is periodic in the rectangle then the product of the slope of the trajectory and aspect ratio of the rectangle is rational. Furthermore, all periodic trajectories of the rectangle have even period.*

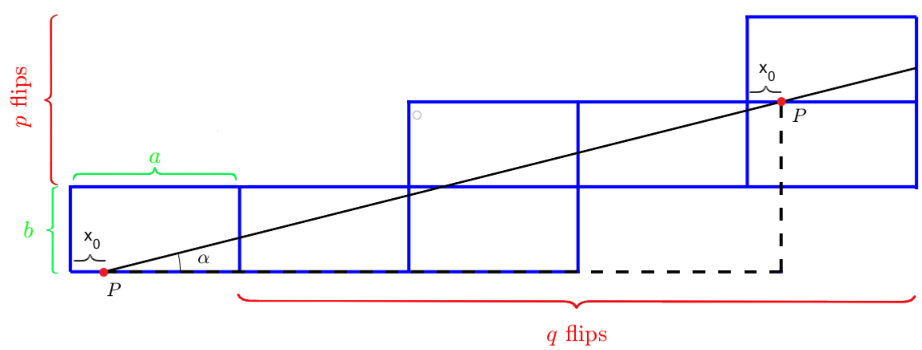

Figure 2.8: Candidate periodic trajectory in $\mathbb{R}^2_R$ with p vertical and q horizontal reflections before returning to the initial position P.

The proof for Proposition 2.12 is almost the same as for Theorem 2.6. Here, the dashed triangle has height pb and base qa, where p and q are the number of vertical and horizontal reflections, respectively. The slope of the trajectory is $\tan(\alpha) = \frac{pb}{qa}$, where $\frac{p}{q} \in \mathbb{Q}$. Rearranging gives the necessary periodicity condition: $\frac{a}{b}\tan(\alpha) = \frac{p}{q} \in \mathbb{Q}$. The period is $p + q$ which is even by the same orientation argument. By Definition 2.7, the period is least if $\gcd(p, q) = 2$. For trajectories with the irrational slope aspect ratio products, these will be uniformly dense (provided they are not pre-images of the vertex).

2.5.1 Construction of periodic orbits within the rectangle

Given a fixed rectangle with side lengths a and b, where $b \leq a$, we are able to construct a least period-T orbit by the following process. We find $p, q \in \mathbb{N}$ such that $T = p + q$ and

$\gcd(p, q) = 2$, for which there are $\varphi(\frac{T}{2})$ unique combinations by Proposition A.1. The initial angle will be chosen such that it satisfies $\alpha = \text{atan}(\frac{pb}{qa})$. Any non-degenerate rectangle will be able to produce all even periodic orbits. The limiting case of a period-2 orbit requires special attention: we take $p = 2$ and $q = 0$. This corresponds to a trajectory with infinite slope: a vertical line. Therefore, $\alpha = \frac{\pi}{2}$ produces a period-2 orbit for all rectangles! However, in general, the angle required will depend on the aspect ratio of the rectangle. For example, a rectangular billiard table with aspect ratio $\frac{a}{b} = \frac{2}{1}$ will generate period-4 trajectories for angles $\text{atan}(\frac{1}{2})$. But an angle of $\text{atan}(\frac{1}{2})$ in a rectangle with aspect ratio $\frac{4}{3}$ produces period-10 orbits.

2.5.2 Vertex pre-images within the rectangle

The results for vertex pre-images in the square also translate over to rectangles. The only difference is that we refer to the product of aspect ratio of the rectangle and slope compared to just the slope in Section 2.4.

Proposition 2.13. *In the rectangle, if a billiard trajectory starts at a vertex where the product of the aspect rational and slope is irrational, then the trajectory never collides with another vertex.*

Corollary 2.14. *In the rectangle, if a billiard trajectory starts at a vertex where the product of the aspect rational and slope is irrational, then the trajectory will always end up in a vertex.*

Proposition 2.15. *In the rectangle, if the billiard trajectory starts at a vertex with a slope that yields period-T orbits when the initial position is not a pre-image of the vertex. Then the order of pre-images is given by $\frac{T}{2} - 2$.*

Remark 2.16. The pre-images of a rectangle with aspect ratio h are proportionally distributed along the side length when compared to a square.

Remark 2.16 follows by applying the linear transform to the pre-image locations. We will make use of this observation in Chapter 5.

2.5.3 Extensions to the parallelogram

It is tempting to apply a more general linear transform to $\mathbb{R}^2_S$ that shears the squares into a parallelogram. Note that this would not correspond to an unfolding process due to asymmetry of an arbitrary parallelogram.

The unfolding technique fails for general parallelograms as many parallelograms may intersect and there will be regions that are uncovered, i.e., an arbitrary parallelogram cannot tessellate the entire plane. In the following chapters we will present a dynamical systems approach that avoids these problems.

Chapter 3

A Dynamical Systems Approach

Mathematical billiards is inherently a dynamical system that describes how the point mass moves/evolves over time. However, the behaviour of billiards is not typically studied with traditional dynamical systems techniques such as bifurcation theory, phase portraits and parameter continuation. Classical billiard theory utilises results from Teichmüller theory and algebraic geometry, which produce elegant results such as in Chapter 2, but are difficult to generalise. In this chapter, we consider a dynamical systems approach despite the fact that billiards exhibit stubbornly degenerate behaviour. The first step is to find a set of equations that model the billiard trajectory from one collision to another collision.

3.1 Our map

For convenience, we now denote the sides AB, BC, CD, DA as sides 0, 1, 2 and 3, respectively. Some figures selectively still use the old notation for clarity purposes. Let us map the four sides of the square onto the interval [0,4). The interval [0,1) represents side 0, which is the base side from which we start any initial condition.The intervals [1,2), [2,3), [2,3) respectively represent sides 1, 2 and 3. Let $P \in [0, 4)$ be the position at which the billiard collides with the boundary. Given a position P, the side is determined by $\lfloor P \rfloor$ where $\lfloor \cdot \rfloor$ is the floor function. Then $\alpha \in (0, \pi)$ is given by the angle between the trajectory after collision and the line segment $\{P + \tau(\lceil P \rceil - P) | \, 0 \leq \tau \leq 1\}$ (anti-clockwise angle with respect to the side), where $\lceil \cdot \rceil$ is the ceiling function.

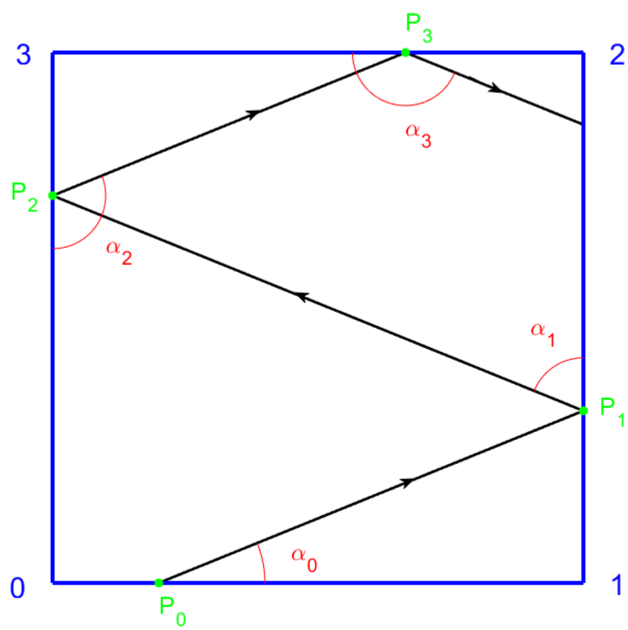

Figure 3.1: Example trajectory depicted with the positions P and angles α for each collision.

We define our map $(\alpha_{n+1}, P_{n+1}) = F(\alpha_n, P_n)$ as follows; the derivation for the case of a parallelogram can be found in the Appendix. For brevity, let $x_n = P_n - \lfloor P_n \rfloor$. Given initial point (α_n, P_n), what is the next side that the trajectory collides with?

$$\lfloor P_{n+1} \rfloor = \begin{cases} \lfloor P_n \rfloor + 1 \pmod 4, & \text{if } \alpha_n \in (0,\, \text{acot}(1 - x_n)), \\ \lfloor P_n \rfloor + 2 \pmod 4, & \text{if } \alpha_n \in (\text{acot}(1 - x_n),\, \pi - \text{acot}(x_n)), \\ \lfloor P_n \rfloor + 3 \pmod 4, & \text{if } \alpha_n \in (\pi - \text{acot}(x_n),\, \pi). \end{cases}$$

Note that the billiard trajectory cannot collide with the same side in succession. For $\alpha = 0$, $\text{acot}(1 - x_n)$, $\pi - \text{acot}(x_n)$, or π, the trajectory terminates at a vertex. We refer to $\lfloor P_n \rfloor + 1 \pmod 4$ as the right-adjacent side, $\lfloor P_n \rfloor + 2 \pmod 4$ as the opposite side, and $\lfloor P_n \rfloor + 3 \pmod 4$ is the left-adjacent side.

The image $(\alpha_{n+1}, P_{n+1}) = F(\alpha_n, P_n)$ depends on whether $\lfloor P_{n+1} \rfloor$ is one of the adjacent sides or the opposite side.

$$\alpha_{n+1} = f(\alpha_n, P_n) := \begin{cases} \frac{\pi}{2} - \alpha_n, & \text{if } \lfloor P_{n+1} \rfloor = \lfloor P_n \rfloor + 1 \pmod 4, \\ \pi - \alpha_n, & \text{if } \lfloor P_{n+1} \rfloor = \lfloor P_n \rfloor + 2 \pmod 4, \\ \frac{3\pi}{2} - \alpha_n, & \text{if } \lfloor P_{n+1} \rfloor = \lfloor P_n \rfloor + 3 \pmod 4. \end{cases}$$

$$P_{n+1} = g(\alpha_n, P_n) := \lfloor P_{n+1} \rfloor + \begin{cases} \tan(\alpha_n)(1 - x_n), & \text{if } \lfloor P_{n+1} \rfloor = \lfloor P_n \rfloor + 1 \pmod 4, \\ 1 - x_n - \cot(\alpha_n), & \text{if } \lfloor P_{n+1} \rfloor = \lfloor P_n \rfloor + 2 \pmod 4, \\ 1 + x_n \tan(\alpha_n), & \text{if } \lfloor P_{n+1} \rfloor = \lfloor P_n \rfloor + 3 \pmod 4. \end{cases}$$

In terms of maps, we have a periodic orbit of period N if $F^{(N)}(\alpha_0, P_0) = (\alpha_0, P_0)$. Note that any given trajectory comprises a maximum of four angles, namely $\{\alpha_0, \frac{\pi}{2} - \alpha_0, \frac{3\pi}{2} - \alpha_0, \pi - \alpha_0\}$.

3.2 Surface representation of our map

The dynamics of the map can be seen through the billiard trajectories within the square which have been presented throughout Chapter 2. We can also investigate the billiard trajectories by studying the graph of the 2D map in $(\alpha_n, P_n, \alpha_{n+1}, P_{n+1})$-space, Figure 3.2 shows a projection of this graph in (α_n, P_n, P_{n+1})-space with the α_{n+1}-coordinate visualised as a colour on the graph. Notice that the surface is divided into disjoint segments according to the current side $\lfloor P_n \rfloor$, and the surface for each side is a vertical shift compared to the others. The modulo 4 operation in our map causes the discontinuity observed for sides $\lfloor P_n \rfloor = 1$ and 2. It suffices only to investigate our surfaces for $\lfloor P_n \rfloor = 1$.

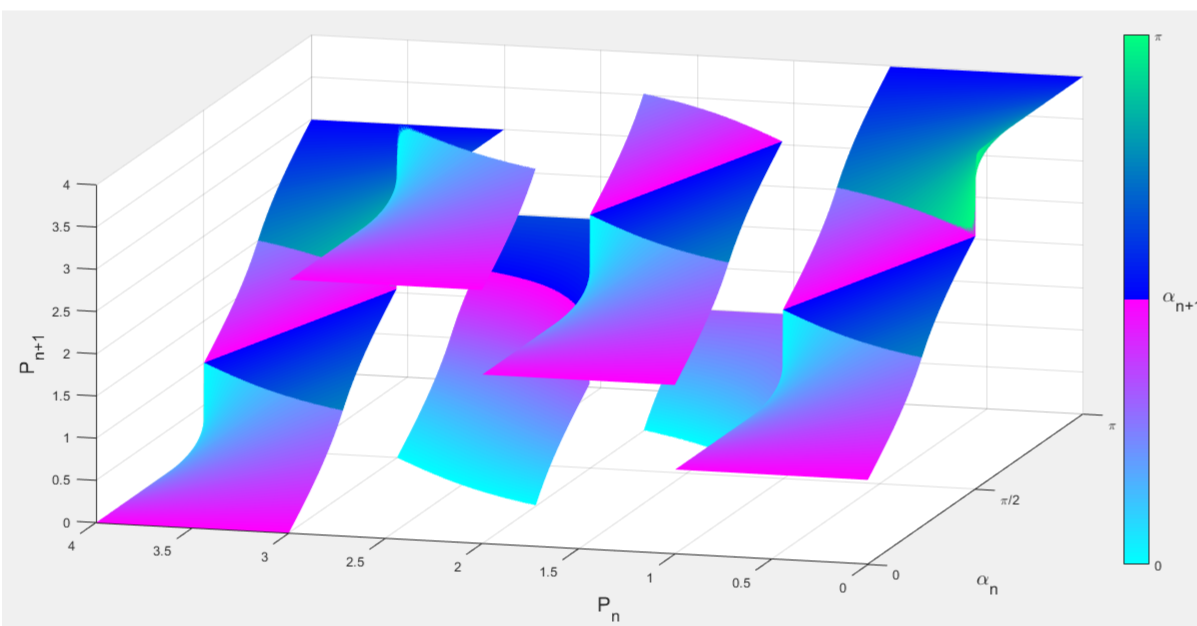

Figure 3.2: Surface plot of (α_n, P_n) against P_{n+1} coloured by α_{n+1}.

The sudden changes in colour on the surfaces indicate the boundary between the different sides. For example, the transition from the pink-cyan segment (corresponding to $0 < \alpha_{n+1} \leq \frac{\pi}{2}$) to the dark-blue segment ($0 < \alpha_{n+1} < \frac{\pi}{2}$) is the boundary between sides 2 and 3. The boundary curves are given by setting $\alpha = \text{acot}(1 - x_n))$ and $\alpha = \pi - \text{acot}(x_n)$. Note that the distinct colour change from dark-blue to cyan for $\lfloor P_{n+1} \rfloor = 2$ is not a boundary transition, it is chosen such that we highlight the transition from $\alpha_{n+1} < \frac{\pi}{2}$ to $\alpha_{n+1} > \frac{\pi}{2}$ because this indicates the direction of the billiard trajectory.

The graph in Figure 3.3 shows the first iterate of our map. By computing our map for N iterations, we can easily generate surfaces to describe P_{n+N} and α_{n+N}, whereas it is extremely tedious to compose our map N times analytically. The intersections between the graph of the Nth iterate and the plane $P_{n+N} = P_n$ are candidate points for a period-N orbit of our map. Note that we also require $\alpha_{n+N} = \alpha_n$, which is not directly visualised in the (α_n, P_n, P_{n+1})-space.

As mentioned earlier, billiards is not traditionally studied with numerical tools from dynamical system theory. In all the billiard textbooks there is no remark regarding the non-existence of odd periodic orbits. Our approach revealed these properties that we subsequently proved in Proposition 2.5 and Theorem 2.6. Using dynamical systems techniques we can also visualise this property for period-3 orbits.

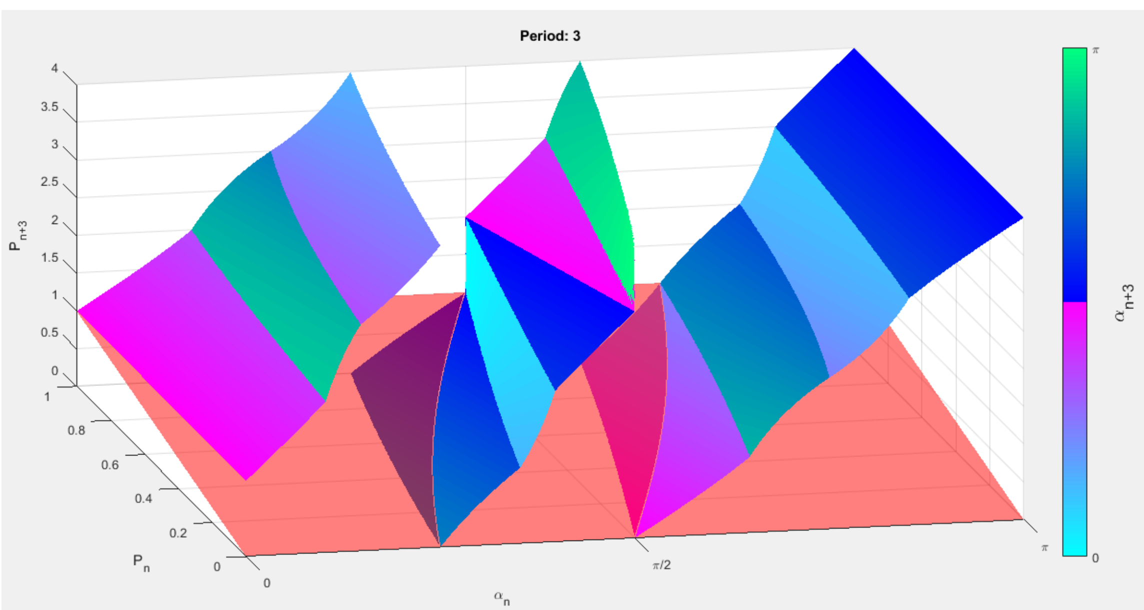

Figure 3.3: Surface plot of (α_n, P_n) against P_{n+3} coloured by α_{n+3}. The transparent red plane is given by $P_n = P_{n+3}$.

Figure 3.3 shows the third iterate of F together with the diagonal plane $P_{n+3} = P_n$ (red transparent plane). From Figure 3.3, we observe that there are two segments of the surface, that return to side 0 after three iterations. These two segments correspond to trajectories going from side $0 \mapsto 1 \mapsto 2 \mapsto 0$ or side $0 \mapsto 3 \mapsto 2 \mapsto 0$. This can be seen via the colour given by α_{n+3} matching $\pi - \alpha_n$, and can be reconstructed with the first iterate shown in Figure 3.2.

The curves of intersection between the plane and our surface imply that $P_n = P_{n+3}$ at these curves. This is a necessary condition for there to exist a period-3 orbit, but not sufficient, because $\alpha_n = \alpha_{n+3}$ is also necessary. We could use a plot with α_{n+3} on the z-axis and examine the intersection with the plane. Instead, we use the colour bar provided in Figure 3.3. Notice that for the left intersection, $\alpha_n < \frac{\pi}{2}$ but $\alpha_{n+3} > \frac{\pi}{2}$. Conversely, for the right intersection, we find that $\alpha_n > \frac{\pi}{2}$ and $\alpha_{n+3} < \frac{\pi}{2}$. In both cases, $\alpha_{n+3} = \pi - \alpha_n$. The limiting case $\alpha_n = \frac{\pi}{2}$ exhibits a period-2 orbit and not a period-3 orbit; note the similarity to the proof by contradiction used in Proposition 2.5. Therefore, this apparent intersection is not a period-3 orbit. Furthermore, there is, in fact, a discontinuity in the surface on the curves where the red plane $P_n = P_{n+3}$ intersects. The two intersection curves are given by iterating our map three times with $\alpha = \text{acot}(1 - x_n)$ and $\alpha = \pi - \text{acot}(x_n)$. These angles give trajectories that pass through the vertex on the first iteration. This result coincides with Proposition 2.11, where a trajectory that revisits an earlier position with angle $\pi - \alpha_n$ must have passed through a vertex.

3.3 Jacobian for our map

In bifurcation theory, the Jacobian provides information on the stability and determines when a bifurcation has occurred.

We can find the Jacobian for a single iteration of the map analytically as

$$DF(\alpha, P) = \begin{bmatrix} \frac{\partial f}{\partial \alpha} & \frac{\partial f}{\partial P} \\ \frac{\partial g}{\partial \alpha} & \frac{\partial g}{\partial P} \end{bmatrix},$$

where $\alpha_{n+1} = f(\alpha_n, P_n)$ and $P_{n+1} = g(\alpha_n, P_n)$ as defined in Section 3.1. Hence, we find the three different cases, namely,

$$DF(\alpha, P) = \begin{cases} \begin{bmatrix} -1 & 0 \\ (1-x)\text{sec}^2(\alpha) & -\tan(\alpha) \end{bmatrix}, & \text{if } \alpha \in (0, \text{acot}(1-x)), \\ \begin{bmatrix} -1 & 0 \\ \text{cosec}^2(\alpha) & -1 \end{bmatrix}, & \text{if } \alpha \in (\text{acot}(1-x),\, \pi - \text{acot}(x)), \\ \begin{bmatrix} -1 & 0 \\ x\text{sec}^2(\alpha) & \tan(\alpha) \end{bmatrix}, & \text{if } \alpha \in (\pi - \text{acot}(x),\, \pi). \end{cases}$$

Suppose we have a period-N orbit where $\{(\alpha_1, P_1), ..., (\alpha_N, P_N)\}$ When our billiard trajectory avoids the vertices, our map is smooth which allows us to find the stability of the periodic orbit as a product of Jacobians from one iteration:

$$DF^{(N)}(\alpha_1, P_1) = \prod_{i=1}^{N} DF(\alpha_i, P_i)$$

The first row of every matrix in the product will be $\begin{bmatrix}-1 & 0\end{bmatrix}$ and periodic orbits within the square have even period; see Section 2.3. Therefore, the resulting product of these matrices must have the first row $\begin{bmatrix}1 & 0\end{bmatrix}$ and the matrix $DF^{(N)}$ is lower triangular with eigenvalue 1 for all periodic orbits. The presence of the eigenvalue 1 implies that our periodic orbits are non-hyperbolic, a degeneracy that is expected because we have a family of periodic orbits (almost any position is sufficient). It is expected that periodic orbits within the square/rectangle are non-hyperbolic. Recall from Chapter 2 that the necessary condition for a periodic orbit in the square is $\tan(\alpha) \in \mathbb{Z}$. Thus, a small perturbation in the angle can qualitatively change a trajectory from periodic to non-periodic.

By computing the finite difference approximations, we find that the Jacobian is independent of the position and that the second row and second column entry is always 1. Hence, it is of the form:

$$DF^{(N)}(\alpha, P) = \begin{bmatrix} 1 & 0 \\ h(\alpha) & 1 \end{bmatrix}.$$

Therefore, our system is highly degenerate as both eigenvalues of the Jacobian are 1. The potential cause for this degeneracy is that our angle does not vary much throughout a billiard trajectory, there is a maximum of four unique angles for any given trajectory within the square and rectangle. We find that orbits with a large number of possible angles, such exist in the parallelogram and the triangle, the second row and second column entry is no longer 1. The bottom left element of $DF^{(N)}(\alpha, P)$ has a value $h(\alpha)$ that depends only on α. We were unable to find a closed formula for $h(\alpha)$, although we think one exists that can be found with two-dimensional induction. For $n, m \in \mathbb{N}$, we perform the first iteration of induction on angles of the form $\alpha = \text{atan}\frac{n-1}{1}$, this is a period-$2n$ orbit where the trajectory collides with the left/right sides of the square twice and the bottom/top sides $2n-2$ times. We can then reorder the product to ensure that the adjacent collisions with the bottom/top occur first and in the middle, the rest of the product consists of matrices from opposite collisions. We then perform induction on m for angles of the form $\alpha = \text{atan}\frac{n-1}{m}$ which would then account for all possible angles.

3.4 Solving the degeneracy dilemma

We aim to examine how the existence of periodic orbits evolve as we change the shape of the table. Parameter continuation is a numerical analysis technique used to study how solutions to dynamical/algebraic systems evolve as parameters are adjusted. We first consider the transition from the square to the rectangle by changing the aspect ratio. We are able to compare our numerical results with the theoretical results from Chapter 2. We then apply the continuation method with minor adjustments from the square to the parallelogram for which little is known.

To find periodic orbits, we reduce our two-dimensional map into a two-dimensional system of non-linear algebraic problems. Then this resolves to a classical root finding problem. The naive first approach is to enforce a fixed point (α, P) for the Nth iterate of the map[1].

$$\begin{cases} f^{(N)}(\alpha, P) - \alpha = 0 \\ g^{(N)}(\alpha, P) - P = 0 \end{cases} \iff F^{(n)}(\alpha, P) - I \begin{bmatrix} \alpha \\ P \end{bmatrix} = 0. \tag{3.1}$$

The solutions to the system of equations (3.1) are non-regular as the Jacobian for our system will be $DF^{(n)}(\alpha, P) - I$ which will always have two zero eigenvalues; see Section 3.3. Therefore, iterative schemes such as Newton's method cannot be used to track the parameter dependent family. The essence is that the problem is not well posed due to existence of an entire family of peridic orbits, since for any given periodic α there exists an infinite number of suitable P. To address this problem, we reformulate the algebraic system such that we isolate one unique periodic orbit and then follow this solution in a system parameter using parameter continuation.

For conservative vector fields and Hamiltonian systems, the conventional method to deal with families of periodic orbits is to reformulate the problem by introducing an additional term. The term is a product of a new parameter multiplied with the derivative of some conserved quantity (eg., the Hamiltonian) [15, 26]. This isolates the periodic orbits to only a single value of the new parameter for which we could then perform parameter continuation. We decided against using this technique for three reasons. Firstly, we have discrete maps rather than the smooth continuous systems considered in the literature. Secondly, our billiard maps are time-reversible and "time-reversible systems form an exceptional class" [26] for which the approach has not been applied yet. Thirdly, for billiards it is difficult to find a candidate conserved quantity since commonly the conserved term is derived from physical arguments such as damping. In the billiard literature, it is known that, for smooth closed $\mathcal{D}$, an area form with the symplectic wedge product is invariant [34]. However no such results apply to non-smooth $\mathcal{D}$ like our quadrilaterals. We suspect this is a major reason why parameter continuation methods have not appeared in billiard literature. It is highly non-trivial as to how to use parameter continuation to study billiards.

While the parameter continuation technique for conserved systems described above follows an entire family of periodic orbits, we propose a novel reformulation which instead selects a particular periodic orbit from the family to follow. We search for a solution measure that

[1] We have omitted the map for the rectangle billiard as it is a special case of the parallelogram map in Section 4.2.

parametrises the family. Our first idea, arclength of a trajectory, does not suffice, because for a given period, the arclength is invariant under the initial position. This can be proven with unfolding as the different trajectories are simply horizontal translations in $\mathbb{R}^2_S$ and, therefore, arclength is preserved.

3.4.1 Area of a periodic orbit

Consider the following motivating example inspired by the pre-images of the vertex in Section 2.4. For a period-6 orbit with $\alpha = \text{atan}(2)$ we find that the only pre-image of the vertex on the base is $P = 0.5$. In Figure 3.4 we depict period-6 orbits with initial conditions $P_0 = 0.25, 0.4, 0.5$. Observe that as P_0 approaches 0.5, the trajectory degenerates into a singular trajectory. Furthermore, the two symmetric bands have an area that is degenerate for $P_0 = 0.5$.

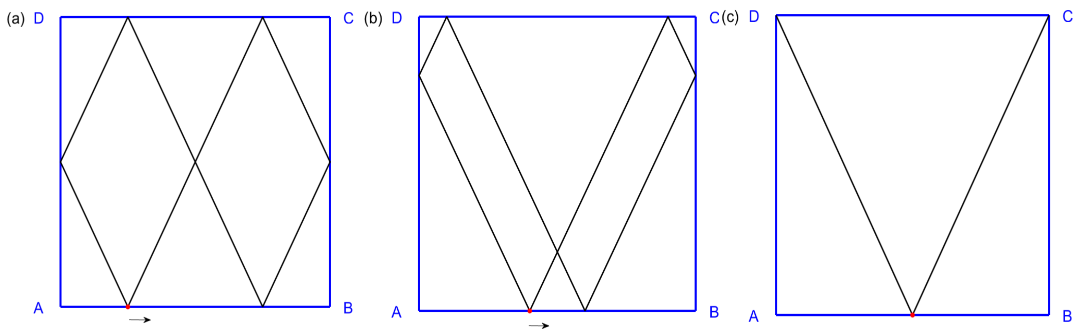

Figure 3.4: Varying the initial position (red dot) of a period-6 orbit with $\alpha_0 = \text{atan}(2)$. Panels (a), (b) and (c) depict initial positions of 0.25, 0.4 and 0.5, respectively.

From the theory provided in Section 2.4, we select the isolated periodic orbit that has maximal area between the "bands". We define a notion of area such that it can be calculated cumulatively based on each iteration of the map rather than using the geometric structure at the end, because this approach extends more readily to higher-order periodic orbits and other boundaries. We propose the following cumulative area function:

Definition 3.1. A period-T orbit that visits positions $\{P_0, \ldots, P_{T-1}\}$, has area $A = T - \sum_{i=0}^{T-1} \tilde{a}_i$, where

$$\tilde{a}_i = \begin{cases} \frac{1}{2}(1-x_i)x_{i+1}, & \text{if } \lfloor P_{i+1} \rfloor = \lfloor P_i \rfloor + 1 \pmod 4, \\ 0, & \text{if } \lfloor P_{i+1} \rfloor = \lfloor P_i \rfloor + 2 \pmod 4, \\ \frac{1}{2}x_i(1-x_{i+1}), & \text{if } \lfloor P_{i+1} \rfloor = \lfloor P_i \rfloor + 3 \pmod 4, \end{cases}$$

and $x_i = P_i - \lfloor P_i \rfloor$.

The values $\tilde{a}_i$ represent an area outside of the bands, so A is maximal when the sum of $\tilde{a}_i$ is minimal. The additional term T ensures that the area A is positive as each cumulative area will be less than the area of the domain. Furthermore, larger periodic orbits and larger shapes are expected to have larger areas. Figure 3.5 gives a geometric interpretation of A. The measure A represents the white area given by the period-6 orbit in the square. Starting from the point on AB closest to B, the trajectory first collides with an adjacent side, and we calculate the area of the red triangle created between the trajectory and the domain. The next step, again creates a red triangle as we hit the side CD. However, the trajectory then moves to the opposite side AB and the cumulative area does not change. We can prove, using the return map in Appendix A.2 for the square, that the sum of the remaining blue and green areas, which are not covered by the adjacent triangles, is invariant for the given family of periodic orbits. In other words, the sum of the blue and green areas in Figure 3.5 is constant for any P on AB.

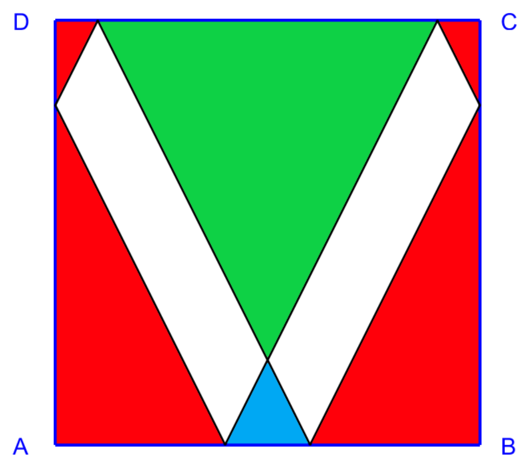

Figure 3.5: Decomposition of the square based on a typical period-6 trajectory. The white area depicts the intended measure of area of the orbit, the red triangles are used in the calculation of the cumulative area and the sum of the blue and green areas are invariant.

Suppose we are interested in a particular period. We know from Chapter 2 the exact angles required to produce an orbit with this period. Our definition of area is maximised when the position is equal to the midpoint between the vertices and pre-images of the vertices. For example, a period-4 orbit in the square requires $\alpha = \frac{\pi}{4}$. By Proposition 2.10, the order of pre-images is 0. Therefore, the midpoint $P = 0.5$ of the vertices leads to a period-4 trajectory that maximises the area. Figure 3.6 shows how A varies with P_0 for the case of a period-4 orbit in panel (a) and a period-10 orbit in panel (b). Note that the area is minimal exactly at the pre-images of the vertices and the vertices; a period-10 orbit with $\alpha = \text{atan}(4)$ will have pre-images of order 3, which are located at 0.25, 0.5 and 0.75. The positions that maximise the area are then the successive midpoints 0.125 , 0.375, 0.625 and 0.875. Note that we will have a problem for period-2 orbits with $\alpha = \frac{\pi}{2}$ as the area is always 1, but it is a limiting case.

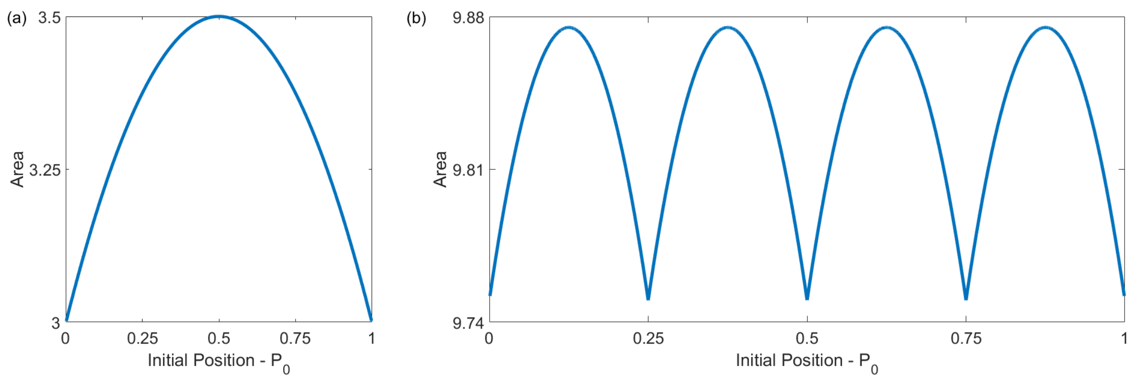

Figure 3.6: Visualisation of the area A from Definition 3.1 as P_0 varies for the case in panel (a) of the period-4 trajectories with fixed $\alpha_0 = \frac{\pi}{4}$ and in panel (b) the period-10 trajectories with fixed $\alpha_0 = \text{atan}(4)$.

Chapter 4

Parameter Continuation Methods

In this chapter we perform parameter continuation by following periodic orbits from the square to the rectangle as a proof of concept. We then perform continuation from the square to the parallelogram which uncovers and motivates surprising and novel results.

4.1 Square to rectangle continuation

In order to follow the periodic orbit with maximal A in the parameter that transforms the square into a rectangle, we add the constraint $\frac{dA}{dP} = 0$ such that the area is maximised; note that the derivative is not defined at the minimum as seen in the non-smooth points in Figure 3.6. However, since we also have the conditions that $f^{(N)}(\alpha, P) - \alpha = 0$ and $g^{(N)}(\alpha, P) - P = 0$, our system is over-determined with three equations and only two unknowns (α, P). We decided to drop the equation for the angle for three reasons. First of all, the equation for α results in a non-invertible Jacobian $DF - I$, for all periodic orbits in the square; see Section 3.3. Secondly, if the position equation is satisfied, we must return with the same angle and have a periodic orbit because after N iterations we cannot have $\pi - \alpha$ by Proposition 2.11 which implies that the angle must be α. Thirdly, by Proposition 2.8 we know from the periodicity condition that there exists a (α, h)-relationship. Therefore, in the square/rectangle, the position equation alone determines periodic orbit solutions and the area optimisation constraint will isolate a particular solution. Note that we have carefully chosen the order of equations with $g^{(N)}(\alpha, P) - P = 0$ first to avoid an eigenvalue 0. Hence, we define the system

$$G(\alpha, P) = 0 \iff \begin{cases} g^{(N)}(\alpha, P) - P = 0 \\ \frac{dA}{dP} = 0 \end{cases} \tag{4.1}$$

We use the iterative scheme of Newton's method for equation (4.1):

$$\begin{pmatrix}\alpha_{k+1}\\ P_{k+1}\end{pmatrix} = \begin{pmatrix}\alpha_k\\ P_k\end{pmatrix} - DG(\alpha_k, P_k)^{-1}G(\alpha_k, P_k),$$

where the Jacobian matrix $DG(\alpha_k, P_k) = \begin{bmatrix}\frac{\partial g^{(N)}(\alpha,P)}{\partial\alpha} & \frac{\partial g^{(N)}(\alpha,P)}{\partial P} - 1\\ \frac{\partial^2 A}{\partial\alpha\partial P} & \frac{\partial^2 A}{\partial P^2}\end{bmatrix}$ is approximated by the central difference method using step-size $h = 10^{-6}$; see Appendix A.3 for details. We determine that our Newton iterations have converged if both the ℓ_2 norm of successive difference and maximum function value lie below 10^{-6} and 10^{-8}, respectively. Continuation is performed as follows. Suppose we want to follow a period-N orbit which is given by the initial point (α^*, P^*) and has maximal area in the square. We then perturb the height of the square to become a rectangle and find the new (α, P) which satisfies equation (4.1) by using Newton's method with the initial guess (α^*, P^*). Once the iterative scheme converges, we perturb the height again and the new seed is the converged point from the previous height. In the sequel, we consider a rectangle with base length 1 and the height is a parameter denoted h which is also the aspect ratio of the rectangle. Parameter continuation yields solution branches for $h > 0$, where we continue from $h = 1$ in both positive and negative directions. We examine the examples of two families of period-10 orbits with initial angle atan(4) and atan($\frac{2}{3}$). For each family, we continue branches starting from the four positions and two positions that maximise the area, respectively; see Figure 3.6(b). The continuation for these initial conditions are illustrated in Figure 4.1. Panel (a) illustrates that P_0 remains constant as the aspect ratio h is varied, whereas α_0 increases as h increases. The precise relationship between α_0 and h can be seen with a projection onto the (α, h)-plane in panel (b), we find that α_0 increases rapidly from 0, as h increases, and quickly converges to $\frac{\pi}{2}$. We will show later that $\alpha_0 = \text{atan}(4h)$ and $\alpha_0 = \text{atan}\left(\frac{2}{3}h\right)$ for the families with initial angle $\tan(4)$ and atan($\frac{2}{3}$), respectively.

The example is representative of the general continuation results from the square to the rectangle: the position is invariant but the angle depends on h. The invariance of P_0 is explained by the fact that the pre-images on the base remain unchanged as h is varied; see Remark 2.16. The exact relation between α_0 and h can be found by using Proposition 2.12: A least period $p + q$ orbit requires $\alpha = \text{atan}(h\frac{p}{q})$ which is observed in the figure. As h increases, we require a steeper α_0 in order to collide with the same proportional position on the sides. Note that we currently use a fixed step-size of 10^{-5}; in future work a variable step size can be implemented that adapts the step size according to the number of Newton iterations or the difference in α in order to improve efficiency.

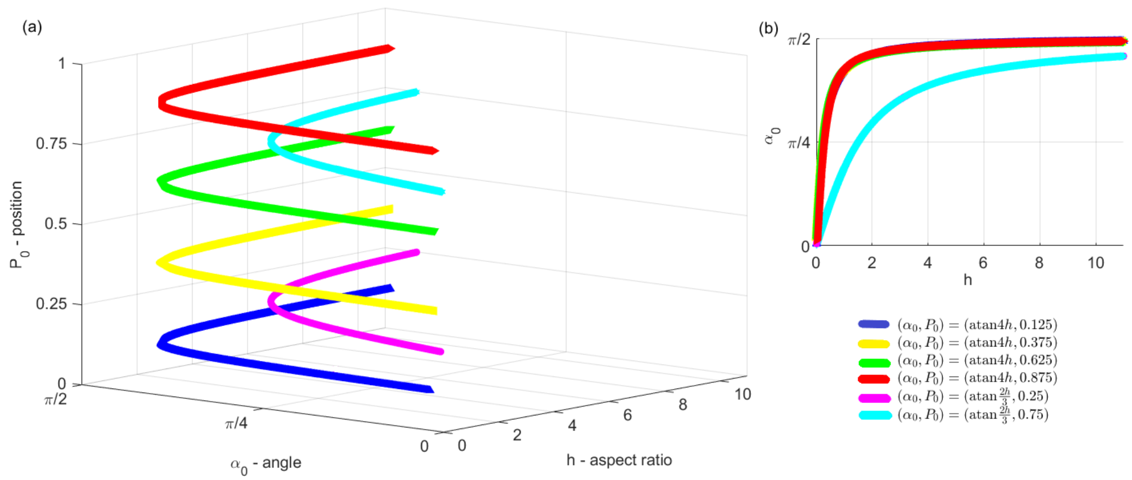

Figure 4.1: Dependence of the initial position and initial angle against the aspect ratio for all period-10 orbits shown in (h, α, P)-space in panel (a) and projection onto (h, α) plane in panel (b).

4.2 Square to parallelogram continuation

The advantage of parameter continuation compared to unfolding and other theoretical tools is that the ideas and code is readily extended onto other problems. We are able to follow periodic orbits from the square/rectangle into the parallelogram with minor adjustments. We uniquely define a general parallelogram with lower left angle γ and height h as depicted in Figure A.2. The explicit formulation of the billiard map within the parallelogram and the derivation can be found in the Appendix.

For parameter continuation, we use the area in Definition A.8 and the system of equations (4.1) except now with two parameters, γ and h. The results from the previous section can be reproduced by varying h while γ remains fixed at $\frac{\pi}{2}$. Hence, even though the setup with fixed h and varying γ will result in convergence of solutions for equation (4.1), however, most will not be periodic orbits as the angle equation is not satisfied. Unlike the square/rectangle, in the parallelogram, we are able to return to the same position but with a different angle. Note that system (3.1) is still ill-posed as the Jacobian is singular, however finite difference approximations to the Jacobian $DF(\alpha, P)$ associated with system (3.1) for the parallelogram, yields one eigenvalue 1. We believe that this is caused by the fact that the angle equation now depends on both α and γ with an implicit dependence on P, there are a greater number of unique angles in a given parallelogram trajectory than a square/rectangle. We perform parameter continuation using the root finding problem (4.1) while monitoring the additional constraint: $f^{(N)}(\alpha, P) - \alpha = 0$. Convergence now requires the ℓ_2 norm of successive differences to be below 10^{-6}, the maximum function value to be below 10^{-8} and satisfying the additional constraint is to within 10^{-6}.

We state some intuitive results regarding small periodic orbits for which the proofs are only slightly more involved than Chapter 2 but are provided in the Appendix A.3.

Proposition 4.1. *There always exists a period-2 orbit for the parallelogram billiard.*

Proposition 4.2. *There do not exist any period-3 orbits for the parallelogram billiard.*

4.2.1 Non-existence of period-4 orbits in the parallelogram

Parameter continuation following the least period-4 orbit in the square with $(\alpha_0, P_0) = (\frac{\pi}{4}, 0.5)$ yields no branch for $\gamma \neq \frac{\pi}{2}$. This suggests that there does not exist any least period-4 orbits for general parallelograms with $\gamma \in (0, \frac{\pi}{2})$. This is a surprising result as the square and rectangular billiards exhibit infinitely many least period-4 orbits. We prove the non-existence using algebraic, geometric and combinatoric arguments. The overview of the proof is as follows: First we argue that, for period-4 orbits, it is sufficient only to consider trajectories that visit the base of the parallelogram; then we account for all combinatoric possibilities of side collisions for period-4 orbits and systemically eliminate them using our parallelogram map or by a geometric contradiction. To assist with our proofs, we denote the sides of the parallelogram with $\lfloor \tilde{P} \rfloor \in \{0, 1, 2, 3\}$ such that the sides AB, BC, CD, DA are 0, 1, 2, 3 respectively.

We define the *cutting sequence* for any periodic orbit as the combinatorial sequence of sides visited by the trajectory [30, 34]. For example, the cutting sequence 0123 corresponds to a trajectory starting from the base and always colliding with the right-adjacent side, the sequence length of four indicates a period-4 orbit. Furthermore, we stipulate that a legal cutting sequence is such that consecutive values in the sequence cannot be the same, because a trajectory cannot re-visit the same side immediately [36]. Note that the notation of some of the proofs follows the derivation of the parallelogram map in Appendix A.3.

Proposition 4.3. *For any parallelogram, a least period-4 orbit cannot have the cutting sequence 0202 or 1313.*

Proof. Suppose for the sake of contradiction that there exists a least period-4 orbit with cutting sequence 0202. Consider a trajectory starting from side 0 at $x_0 = P_0$ where $x_i = P_i = \lfloor \underset{\sim}{P_i} \rfloor$ and with initial angle α_0. Using the parallelogram map, the cutting sequence 0202 corresponds to:

$$\begin{cases} x_{i+1} = 1 - x_i + h(\cot(\gamma) - \cot(\alpha_0)), \\ \alpha_{i+1} = \pi - \alpha_i, \end{cases}$$

where $i = 0, 1, 2, 3$. Back substituting and using the cotangent sum identity yields:
$x_4 = x_0 + 4h\cot\alpha_0$. Enforcing the necessary period-4 condition $x_4 = x_0$ gives $\alpha_0 = \frac{\pi}{2}$ which

is a least period-2 orbit; a contradiction. Using an analogous argument for the 1313 sequence provides the same conclusion. □

An immediate consequence of Proposition 4.3 is that a period-4 orbit must involve collisions with adjacent sides. This implies that it is sufficient to consider only trajectories that start from side 0 of the parallelogram. Furthermore, in order for our cutting sequence to be legal, the first number in our cutting sequence is 0 which implies that the second and fourth numbers cannot be 0.

Lemma 4.4. *For any parallelogram, the cutting sequences 010, 101, 232, 323 are impossible.*

Proof. Suppose for the sake of contradiction that the cutting sequence 010 exists. Consider a trajectory starting from side 0 at $x_0 = P_0$ where $x_i = P_i = \lfloor \underset{\sim}{P_i} \rfloor$ and with $\alpha_0 \in \left(0, \operatorname{atan}\frac{h}{1-x_0+h\cot\gamma}\right)$ such that we collide with side 1. Then according to our parallelogram map: $\alpha_1 = \gamma - \alpha_0 < \gamma$. But in order for the trajectory to travel from side 1 back to side 0, the map requires $\alpha_1 \in (\alpha'_m, \pi)$ where α'_m satisfies $\frac{\sin(\gamma+\alpha'_m)}{\sin(\alpha'_m)} = -x_0$. Lemma A.5 implies that $\alpha'_m \in (\pi-\gamma, \pi)$ which requires $\gamma \leq \alpha'_m < \alpha_1$; hence, we have a contradiction. The proof for the other three sequences follow the same argument. □

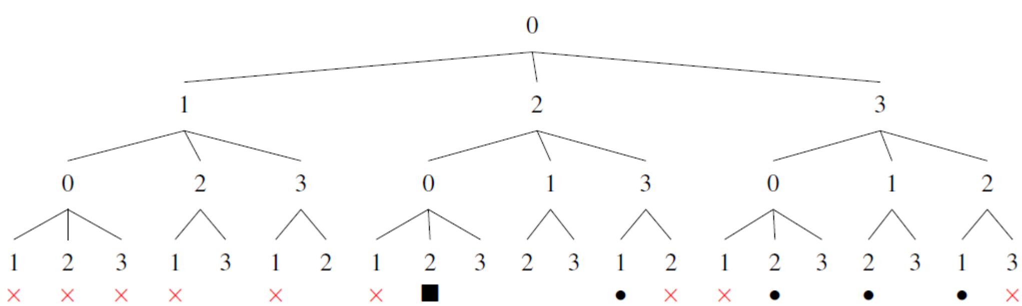

Figure 4.2: A branched tree showing every legal period-4 cutting sequence starting from side 0. The symbols underneath indicate why each sequence cannot yield a period-4 orbit.

Figure 4.2 shows a branched tree depicting all the legal cutting sequences for a period-4 orbit. All sequences that include 010, 101, 232, 323 are impossible by Lemma 4.4, these are marked with a × underneath. Note that the cutting sequence 0301 includes 010 as for a period-4 orbit the starting side is arbitrary. Therefore, the sequence 0301 is equivalent to 3010 which includes the illegal 010. The black square ■ indicates that the trajectory 0202 is impossible because of Proposition 4.3. For the remaining eleven possible sequences, we only need to consider seven of these by using time-reversal symmetry. The sequences 0231, 0302, 0312, 0321 (marked with • underneath) are period-4 if and only if 0132, 0203, 0213, 0123 are period 4, respectively. Hence it remains to show that the seven unmarked sequences cannot be period-4.

Lemma 4.5. *For a parallelogram with $\gamma \in (0, \frac{\pi}{2})$, the cutting sequences 0123, 0203, 0212, 0303, 0313 cannot yield period-4 orbits.*

Proof. We show for these sequences that the angle after four iterations of the parallelogram map does not coincide with the initial angle. For the cutting sequence 0123; $\alpha_1 = \gamma - \alpha_0$, $\alpha_2 = \pi - \gamma - \alpha_1$, $\alpha_3 = \gamma - \alpha_2$ and $\alpha_4 = \pi - \gamma - \alpha_3$. Then $\alpha_4 = 2\pi - 4\gamma + \alpha_0 = \alpha_0$. Hence, the angle only matches for the square/rectangle special case with $\gamma = \frac{\pi}{2}$. Using an analogous argument for the other cutting sequences we find that these only satisfy $\alpha_0 = \alpha_4$ when $\gamma = 0$. $\square$

Note that the two remaining cutting sequences of 0132 and 0213 pass this angle matching test. We employ a geometric argument to demonstrate that these final two sequences cannot be period-4 orbits.

Proposition 4.6. *For a parallelogram with $\gamma \in (0, \frac{\pi}{2})$, the cutting sequences 0132 and 0213 cannot be a period-4 orbit.*

Proof. Suppose for the sake of contradiction that there exists a period-4 orbit with cutting sequence 0132. This will take the form depicted in Figure 4.3 where the angles of reflection are successively denoted by α, β, ϵ and θ. The positions of the collisions are given by P_0, P_1, P_2, P_3 and the trajectory lines intersect at the point denoted O. By $\triangle P_0BP_1$ and $\triangle P_2DP_3$, we get $\gamma = \alpha + \beta$ and $\gamma = \theta + \epsilon$, respectively. As AB and BC are lines, $\angle OP_0P_1 = \pi - 2\alpha$ and $\angle P_0P_1O = \pi - 2\beta$. Using $\triangle OP_0P_1$, gives $\angle P_0OP1 = 2\alpha + 2\beta - \pi$. Then, with $\square AP_2OP_0$, we find that $\angle P_0OP_2 = 2\pi - \gamma - \alpha - \epsilon$. However, $\angle OP_0P_2 = 2\pi - 2\alpha - 2\beta$, because the trajectory is a straight line. Comparing the two expressions for $\angle OP_0P_2$ yields $\beta = \frac{1}{2}(\gamma - \alpha + \epsilon)$. Combining this result with $\triangle P_0BP_1$ gives $\epsilon = \gamma - \alpha$. Then we use $\square P_1CP_3O$ to conclude $\angle P_1OP_3 = 2\pi - \theta - \gamma - \beta$, and via alternate angles we find $\angle P_0OP_2 = \angle P_1OP_3 \implies 2\alpha + 2\beta = \theta + \gamma + \beta \implies \theta = \alpha + \frac{\beta - \gamma}{2}$. Combining this result with $\triangle P_2DP_3$ gives $\gamma - \epsilon = \alpha + \frac{\beta-\gamma}{2}$. Substituting $\epsilon = \gamma - \alpha$ yields $\alpha = \alpha + \frac{\beta-\gamma}{2} \implies \beta = \gamma$. This implies $\alpha = 0$ by using $\triangle P_0BP_1$, which corresponds to the trajectory terminating in vertex B and is clearly not a period-4 orbit. This proof extends to the cutting sequence 0213 by a reflection in the vertical axis. $\square$

Theorem 4.7. *There do not exist any least period-4 orbits for the parallelogram billiard with $\gamma \in (0, \frac{\pi}{2})$.*

Proof. In Propositions 4.3, 4.6 and Lemmas 4.4, 4.5 we account for all legal period-4 cutting sequences and show that all these sequences cannot support a period-4 orbit in a parallelogram with $\gamma \in (0, \frac{\pi}{2})$. $\square$

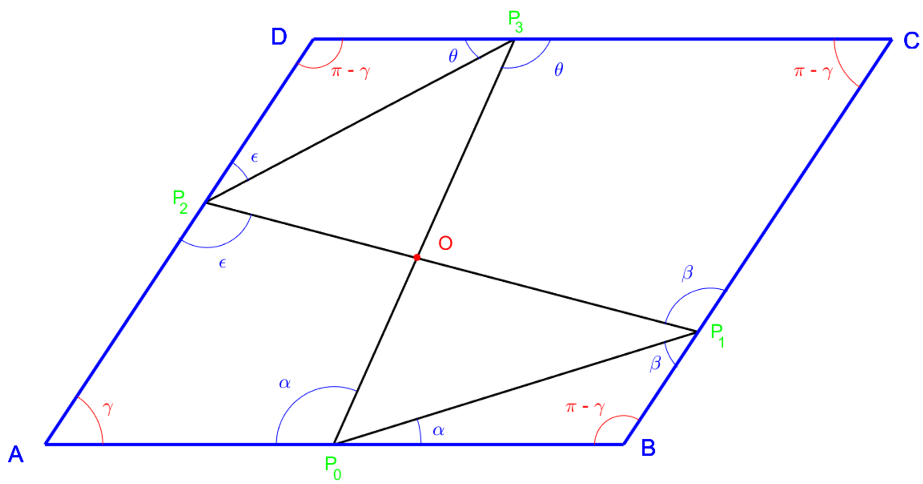

Figure 4.3: Candidate period-4 orbit with cutting sequence 0132 in a parallelogram with lower left angle γ. The angles α, β, ϵ and θ are given by the law of reflection.

4.2.2 Period-6 and higher orbits

We are able to follow period-6 orbits from the square/rectangle into the parallelogram. We are able to continue the branch from initial points $\alpha_0 = \text{atan}(2)$ and $P_0 = 0.25$ or 0.75 and find that both branches cease to exist when the trajectory collides with the vertex. Unlike rectangular billiards, where periodicity (almost) exclusively depends on the initial angle, the position plays a much greater role in the parallelogram. The continuation is best understood with an animation [8], in the left panels of Figure 4.4 we display snapshots of the animation at $\gamma = \frac{\pi}{2}$, 1.5022, 1.4336, 1.3651. As we progress downwards, we find that the trajectory tends towards vertices B and D resulting in a singular trajectory; the continuation terminates at $\gamma_c \approx 1.3651$. In the right panels of Figure 4.4, we plot P_0 on the horizontal and P_6 on the vertical axis. Period-6 orbits lie on the blue line $P_0 = P_6$, the red segments display $g^{(6)}(\alpha_0, P_0)$. Therefore, if a red point lies on $P_0 = P_6$, it may potentially be a period-6 orbit. Observe that as γ decreases from $\frac{\pi}{2}$, the number of positions that possibly support a period-6 orbit for the same α_0 decreases. For $\gamma = \gamma_c + \epsilon$, where $0 < \epsilon << 1$, only $P \approx 0.4724$ supports a period-6 orbit. Inspection of Figure 4.4 suggests that there is a location on the side BC which may support a period-6 orbit as $P_0 = P_6$. For $\gamma = 1.3651$, the intersection occurs at $P_0 = 1.15$, however we check that it is not a period-6 orbit as $\alpha_0 \neq \alpha_6$. We conclude that the class of period-6 orbits born from $\alpha_0 = \text{atan}(2)$ on sides AB cease to exist for $\gamma < \gamma_c$ as the parameter continuation covers all the values of P_0.

The other class of period-6 orbits that we can follow is with initial points $\alpha_0 = \text{atan}(\frac{1}{2})$ and $P_0 = 0.5$. Notice that in the square, this family is simply a 90-degrees clockwise rotation of the previous family, however this relationship does not generalise into the parallelogram. The

solution branch of period-6 orbits terminates when the trajectory collides with vertices B and D; this occurs at $\gamma_c \approx 1.3592$ which is slightly lower than the other period-6 family, nevertheless the behaviour is identical. At γ_c we find that no other positions can support a period-6 orbit.
For the higher periodic orbits we observe similar results, parameter continuation fails to advance once the trajectory has collided with a vertex. Furthermore we also find that once the critical value γ_c is attained, no other points on the parallelogram support the periodic orbit. As the period increases, γ_c increases indicating that the periodic orbit exists for a smaller range of γ. The results for higher periodic orbits are summarised in the following table.

Period	α_0	P_0	γ_c
6	atan(2)	1/4	1.3651
6	atan(1/2)	1/2	1.3592
8	atan(3)	1/6	1.4378
8	atan(1/3)	1/2	1.4378
10	atan(4)	1/8	1.4296
10	atan(1/4)	1/2	1.5117
10	atan(3/2)	1/2	1.4929
10	atan(2/3)	1/4	1.4927

Table 4.1: Results from following orbits with a given period. Columns two to four show, respectively, α_0, P_0 and the minimum γ_c at which continuation with γ terminates.

4.2.3 Period-adding bifurcations

Our parallelogram map is piecewise smooth and piecewise continuous (smooth and continuous on finitely many intervals). These maps typically exhibit border-collision bifurcations when fixed points/periodic orbits cross a discontinuous point or a point where the derivative does not exist [27]. Qualitatively, once the parameter crosses a discontinuity the period changes in an additive manner rather than multiplicative such as in the case of period-doubling bifurcation for continuous maps; this gives rise to the name *period-adding bifurcation*. The theory for continuous piecewise-smooth maps require (typical) periodic orbits/fixed points where the Jacobian cannot have eigenvalues $+1$ or -1 (non-hyperbolic) [27]. As quoted from [4]: "little work has been reported on the analysis of discontinuous maps, which are becoming the subject of increasing scientific interest."

We find that we can observe a sequence of period-adding bifurcations by continuation from the square billiard with $\gamma = \frac{\pi}{2}$ of a period-2 orbit with $(\alpha_0, P_0) = (\frac{\pi}{2}, 3.5)$; in this sequence, each time the trajectory collides with a vertex (discontinuity), the period increases by $+4$. This

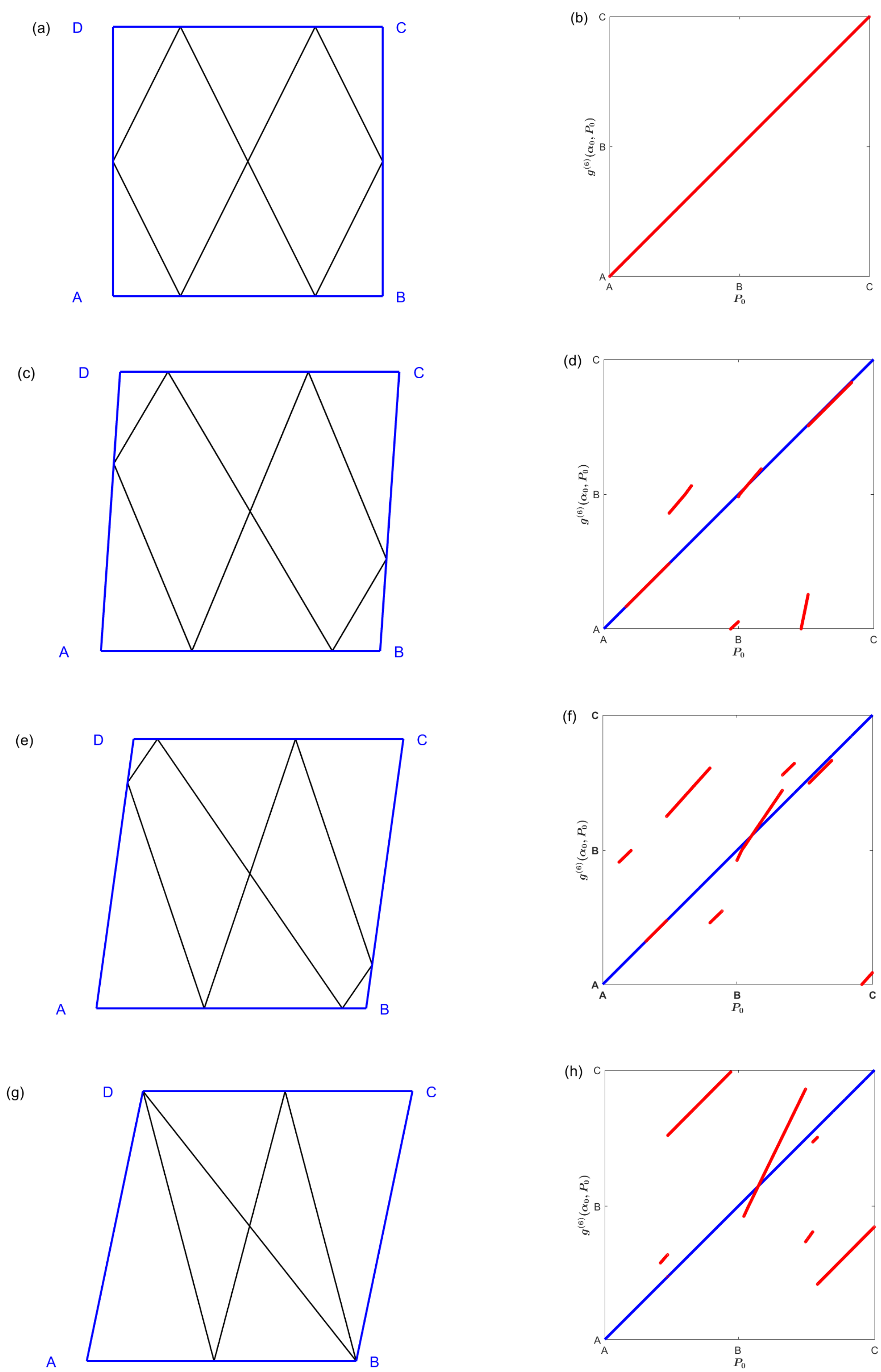

Figure 4.4: The left panels depict parameter continuation of a period-6 trajectory. The right panel shows the 6th iterate of the position map g against the initial position for various P_0 and α_0 is determined by the parameter continuation. Each row corresponds to snapshots are taken at $\gamma = \frac{\pi}{2}$, 1.5022, 1.4336, 1.3651. See also [8] for an animation of this process.

process is best visualised with an animation [8]. A snapshot of eight different γ-values is provided in Figure 4.6, where γ decreases for panels (a) to (h). Starting from the square, we find that the period-2 trajectory tends towards vertex D and bifurcates into a period-6 orbit after the collision with vertex D; see panels (a)-(c). The period-6 trajectory starts with $\alpha_0 = \frac{\pi}{2}$ but the initial position has jumped onto CD. Furthermore, these orbits retrace the same path in the opposite direction. In panels (d)-(e), γ decreases further such that the period-6 trajectory collides with vertices B and D, resulting in a period-10 trajectory. The period-10 trajectory then collides with the vertices to produce a period-14 orbit in panels (g)-(h). With each vertex collision, the trajectory continues onwards with two additional collision points on the angled sides BC and DA; due to the retracing nature of this particular class of periodic orbits, the period then increases by 4.

We used the following trick in order to follow trajectories through vertex collisions. We start the continuation from a very high period, since a period-N orbit is also a period-kN orbit where $k \in \mathbb{N}$, this exploits the fact that non-least periodic orbits still satisfy system (4.1). We note that this trick still fails to follow the generic periodic orbits through the vertices, as in Section 4.2.2. We suspect that a reason why we are able to follow these non-generic periodic orbits through vertices is because the class of periodic orbits exist for all γ [1]. Intuitively as γ decreases, there will exist another periodic orbit of the same class with a larger period dictated by the period-adding bifurcation.

Figure 4.5(a) provides a bifurcation diagram showing the relationship between γ and the positions visited of the periodic orbit, the vertical axis corresponds to the positions visited by the trajectory. The positions of the vertices are depicted with the red lines. The existence and death of each period can be seen with the intersection of the positions visited and red lines. We find cascading behaviour: as γ decreases, the region of existence for each periodic orbit shrinks accordingly; see also Figure 4.5(b). Figure 4.5(a) displays the relationship between γ and the period. Observe that as γ decreases, the period increases and forms an envelope that depicts the minimum and maximum γ which can support a particular period. Upon examination, this appears to resemble a log-log relationship between γ and the period. We note that if the length of the sides of the parallelogram is kept constant, rather than its height, the position remains in the interval $[0, 4)$. With this setup, vertex D always lies to the left of vertex B and we are unable to continue to more slanted parallelograms. Hence, we are not able to observe the sequence of period-adding bifurcations, because this requires the increasing slant, which increases the range of positions $[0, 2+\frac{2}{h\sin\gamma})$ to fit the higher periodic orbits.

[1] the positions that support the periodic orbit do not vanish as we collide with the vertex in the case of the generic orbits in the previous section, this is further discussed in the Appendix.

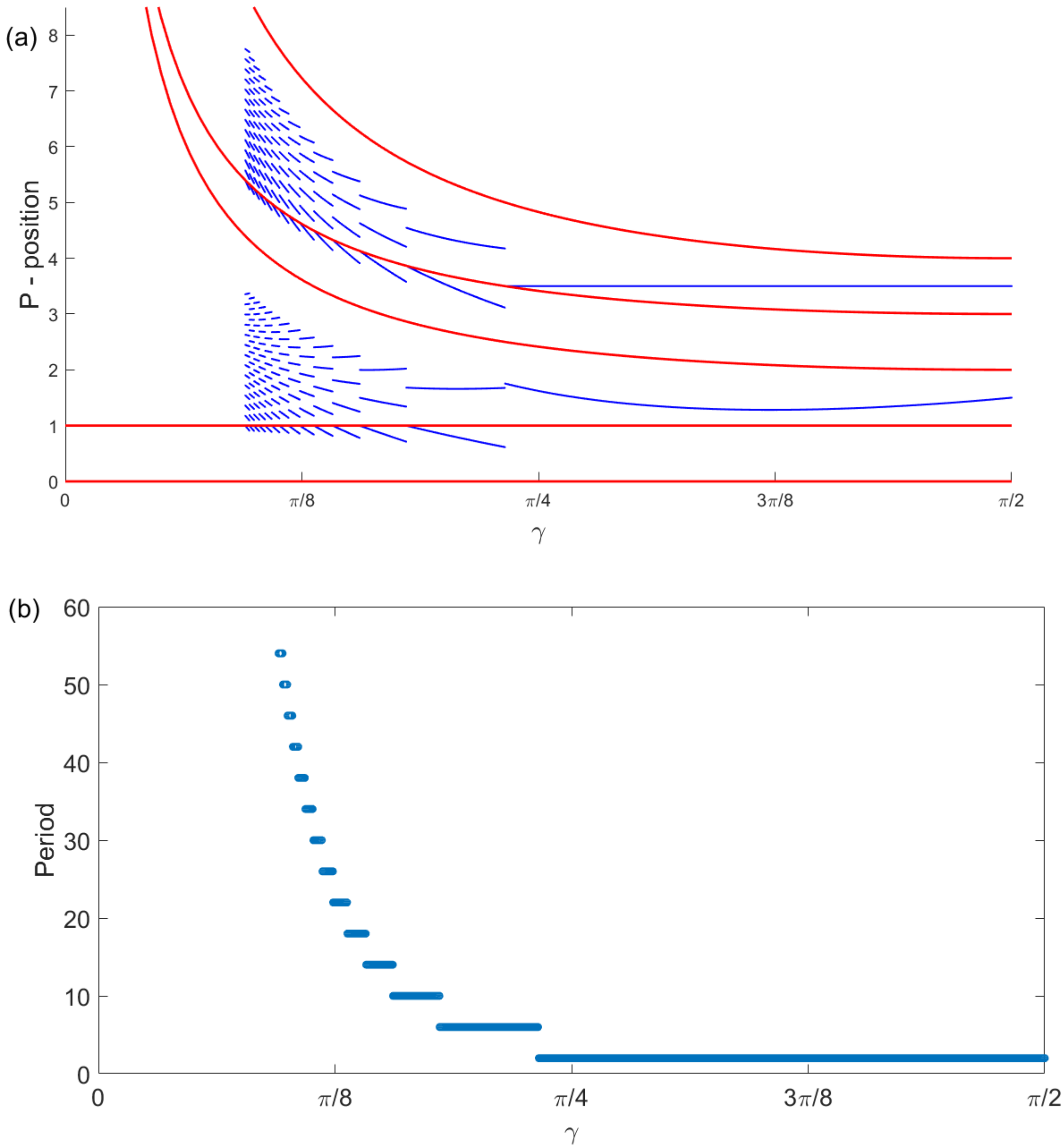

Figure 4.5: Panel (a) shows the sequence of period-adding bifurcations in the (γ, P)-plane; the blue and red curves indicate the positions visited by the periodic orbit and the locations of the vertices, respectively. Panel (b) illustrates the intervals of γ and the periods they support. In both panels computations were done up to period-54, that is, $\gamma = 0.2988$.

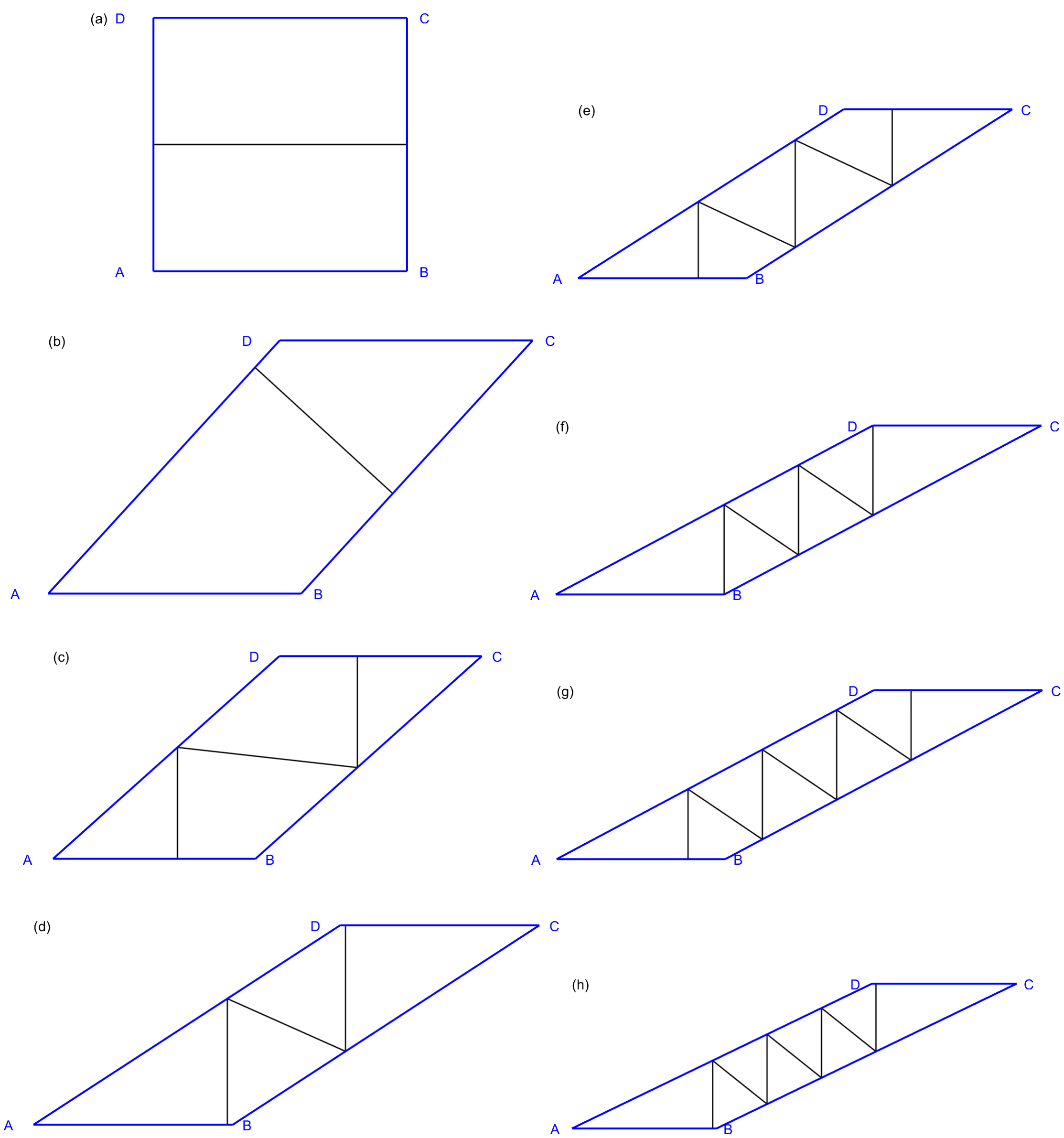

Figure 4.6: Period-adding $(+4)$ bifurcation within the parallelogram. The parameter γ decreases from panels (a) to (h). Panels (a)-(b) depict a period-2 orbit, (c)-(d) a period-6 orbit, (e)-(f) a period-10 orbit and (g)-(h) a period-14 orbit. See also [8] for an animation of this process.

Chapter 5

Conclusion

In this dissertation, we examined billiards within quadrilaterals. In particular we presented theoretical results on periodic orbits within squares and rectangles using classical billiard theory. We presented a dynamical systems approach which confirms the earlier results and is then used to study the parallelogram for which little is known. Parameter continuation inspired a proof for the non-existence of least period-4 orbits in the parallelogram and the existence of a sequence of period-adding bifurcations. Future work would entail finding an analytical proof for this sequence of bifurcations. We only found proofs for very special cases of piecewise-continuous maps which assume linearity and injectivity [20, 22, 23].

The original goal of the project was to investigate the 200-year old open problem regarding triangular billiards. It is more challenging to perform parameter continuation in the triangle as we know very few periodic orbits within the triangle from which we could start the continuation. Interestingly, the periodic orbits found in the parallelogram (Section 4.2.3) which retrace the same path in the opposite direction is reminiscent of one of the very few known periodic orbits which exist in the triangle and also have $\alpha_0 = \frac{\pi}{2}$ [31, 34]. Since triangles are bisections of quadrilaterals, if we can prove the existence of periodic orbits in all quadrilaterals we may be able to find a homeomorphism between any triangle and quadrilateral. Another intriguing approach would be to use parameter continuation follow periodic orbits from a quadrilateral and collapse one of the vertices in order to form a triangle. There is much more to be explored but the early results from our dynamical systems approach yield exciting prospects for future work.

References

[1] B. R. Baer, F. Gilani, Z. Han, and R. Umble. “Periodic orbits on a 120-isosceles triangle-rhombus,120-kite, and 30-right triangle.” (2019). arXiv: 1911.01397.

[2] M. Baker. “Alhazen’s problem”. *American Journal of Mathematics* 4 (1881), pp. 327–331.

[3] A. M. Baxter and R. Umble. “Periodic orbits for billiards on an equilateral triangle”. *The American Mathematical Monthly* 115.6 (2008), pp. 479–491.

[4] M. Bernardo, C. Budd, A. R. Champneys, and P. Kowalczyk. *Piecewise-Smooth Dynamical Systems: Theory and Applications*. Springer-Verlag, 2008.

[5] M. Boshernitzan, G. Galperin, T. Krüger, and S. Troubetzkoy. “Periodic billiard orbits are dense in rational polygons”. *Transactions of the American Mathematical Society* 350 (1998), pp. 3523–3535.

[6] L. A. Bunimovich and C. P. Dettmann. “Open circular billiards and the Riemann hypothesis”. *Physical Review Letters* 94 (2005), pp. 100–201.

[7] N. Burq and M. Zworski. “Bouncing ball modes and quantum chaos”. *SIAM Review* 47.1 (2005), pp. 43–49.

[8] H. H. Chen. *Mathematical billiards: Periodic orbits within quadrilaterals animations*. 2020. URL: https://bit.ly/35Sh7Nx.

[9] H. H. Chen. *Quadrilateral billiards code*. 2020. URL: github.com/HongjiaHChen/QuadrilateralBilliards.

[10] N. Chernov and R. Markarian. *“Chaotic Billiards”*. Vol. 127. American Mathematical Society. Mathematical Surveys and Monographs, 2006.

[11] D. Davis. *“Lines in positive genus: An introduction to flat surfaces, Dynamics done with your bare hands”*. European Mathematical Society Series of Lecture Notes, 2017.

[12] L. DeMarco. “The conformal geometry of billiards”. *Bulletin of the American Mathematical Society* 48 (2011), pp. 33–52.

[13] C. P. Dettmann. “Diffusion in the Lorentz gas”. *Communications in Theoretical Physics* 62 (2014), pp. 521–540.

[14] C. P. Dettmann. “Recent advances in open billiards with some open problems”. *In Frontiers in the Study of Chaotic Dynamical Systems with Open Problems:* 16 (2011), pp. 195–218.

[15] E. J. Doedel, R. C. Paffenroth, H. B. Keller, D. J. Dichmann, J. Galán-Vioque, and A. Vanderbauwhede. “Computation of periodic solutions of conservative systems with application to the 3-body problem”. *International Journal of Bifurcation and Chaos* 13 (2003), pp. 1353–1381.

[16] E. Fredkin and T. Toffoli. “Conservative logic”. *International Journal of Theoretical Physics* 21.3 (1982), pp. 219–253.

[17] G. Galperin. “Playing pool with π (the number π from a billiard point of view)”. *Regular and Chaotic Dynamics* 8.4 (2003), pp. 375–394.

[18] P. M. Gruber. “Convex billiards”. *Geometriae Dedicata* 33.2 (1990), pp. 205–226.

[19] E. Gutkin. “Billiard dynamics: An updated survey with the emphasis on open problems”. *Chaos: An Interdisciplinary Journal of Nonlinear Science* 22.2 (2012), p. 026116.

[20] P. Jain and S. Banerjee. “Border-collision bifurcations in one-dimensional discontinuous maps”. *International Journal of Bifurcation and Chaos* 13.11 (2003), pp. 3341–3351.

[21] A. Katok. *Five most Resistant Problems in Dynamics*. Berkeley September: MSRI-Evans Lecture, 2004.

[22] A. Kumar, S. Banerjee, and D. P. Lathrop. “Dynamics of a piecewise smooth map with singularity”. *Physics Letters A* 337.1 (2005), pp. 87–92.

[23] T. LoFaro. “Period-adding bifurcations in a one parameter family of interval maps”. *Mathematical and Computer Modelling* 24.4 (1996), pp. 27–41.

[24] P. Loomis, M. Plytage, and J. Polhill. “Summing up the Euler φ function”. *The College Mathematics Journal* 39.1 (2008), pp. 34–42.

[25] J. Mather. “Glancing billiards”. *Ergodic Theory and Dynamical Systems* (1982), pp. 397–403.

[26] F. J. Muñoz-Almaraz, E. Freire, J. Galán, E. Doedel, and A. Vanderbauwhede. “Continuation of periodic orbits in conservative and Hamiltonian systems”. *Physica D: Nonlinear Phenomena* 181 (2003), pp. 1–38.

[27] H. E. Nusse and J. A. Yorke. “Border-collision bifurcations including ‘period two to period three’ for piecewise smooth systems”. *Physica D: Nonlinear Phenomena* 57.1 (1992), pp. 39–57.

[28] E. K. Petersen. *“Ergodic Theory”*. Camridge University Press, 1983.

[29] B. Polster and M. Ross. *Math Goes to the Movies*. Johns Hopkins University Press, 2012.

[30] U. Rozikov. *"An Introduction to Mathematical Billiards"*. World Scientific Publishing Company, 2018.

[31] R. E. Schwartz. "Obtuse triangular billiards II: One hundred degrees worth of periodic trajectories". *Experimental Mathematics* 18.2 (2009), pp. 137–171.

[32] M. Sieber and F. Steiner. "Classical and quantum mechanics of a strongly chaotic billiard system". *Physica D: Nonlinear Phenomena* 44.1 (1990), pp. 248–266.

[33] S. H. Strogatz. *"Nonlinear Dynamics and Chaos: With Applications to Physics, Biology, Chemistry, and Engineering"*. CRC Press, 2018.

[34] S. Tabachnikov. *Geometry and billiards*. American Mathematical Society Student Mathematical Library Vol. 30., 2005.

[35] G. Tokarksy. "An impossible pool shot?" *SIAM Review* 37 (1995), pp. 107–109.

[36] G. Tokarsky, J. Garber, B. Marinov, and K. Moore. *One hundred and twelve point three degree theorem.* 2018. arXiv: `1808.06667`.

[37] S. Tomsovic and J. E. Heller. "Long-time semiclassical dynamics of chaos: The stadium billiard". *Physical Review E* 47.1 (1993), pp. 282–299.

[38] H. Waalkens, J. Wiersig, and H. R. Dullin. "Elliptic quantum billiard". *Annals of Physics* 260.1 (1997), pp. 50–90.

Appendix

Animations discussed in Chapter 4 can be found on Youtube [8].
All the code and documentation can be found on Github [9].

A.1 Euler totient function

Proposition A.1. *The number of tuples (m, n) such that $m, n \in \mathbb{N}$, gcd$(m, n) = 1$ and $N = m + n$ is equal to $\varphi(N)$, Euler's totient function evaluated at N.*

Proof. For any $m, n \in \mathbb{N}$, where $N = m + n$ we have $\gcd(m, n) = \gcd(m, N)$. Since the ordered pair (m, n) satisfies $\gcd(m, n) = 1$, we must also have $\gcd(m, N) = 1$. Therefore, m is a totative of N and the number of ordered pairs is given by the number of totatives, $\varphi(N)$. $\square$

Corollary A.2. *For $T = 2N$, there are $\varphi(N)$ unique angles in the interval $(0, \frac{\pi}{2}]$ that produce a period-T trajectory within the square billiard.*

A.2 Square return map

We construct a return map which determines when the trajectory revisits the base side. We will use the notation from Chapter 2, where the base is denoted as side AB. Recall that $\mathbb{R}^2$ is covered by vertical and horizontal shifts with even magnitude of $\mathbb{K}_2$. The map $x = \tilde{x} \bmod 2$, $y = \tilde{y} \bmod 2$ is surjective with $(\tilde{x}, \tilde{y}) \in \mathbb{R}^2$ and $(x, y) \in \mathbb{K}_2$.

Proposition A.3. *For a trajectory leaving the base side in $\mathbb{K}_S$ with $\alpha \in (0, \frac{\pi}{2})$ and position x_0, the next return position on the base in $\mathbb{K}_2$ is given by:*

$$x_1 = x_0 + 2\cot(\alpha) \pmod 2.$$

Proof. Consider a trajectory starting from position $x_0 \in (0, 2)$ on the base with angle $\alpha \in (0, \frac{\pi}{2})$. Then, the position in $\mathbb{R}^2$ is $x_0 = \tilde{x}_0$. In $\mathbb{R}^2$, the trajectory will revisit the base when we $\tilde{y} = 2k$, for $k \in \mathbb{N}$. The first revisit occurs when $\tilde{y} = 2$; see Figure A.1. Using the

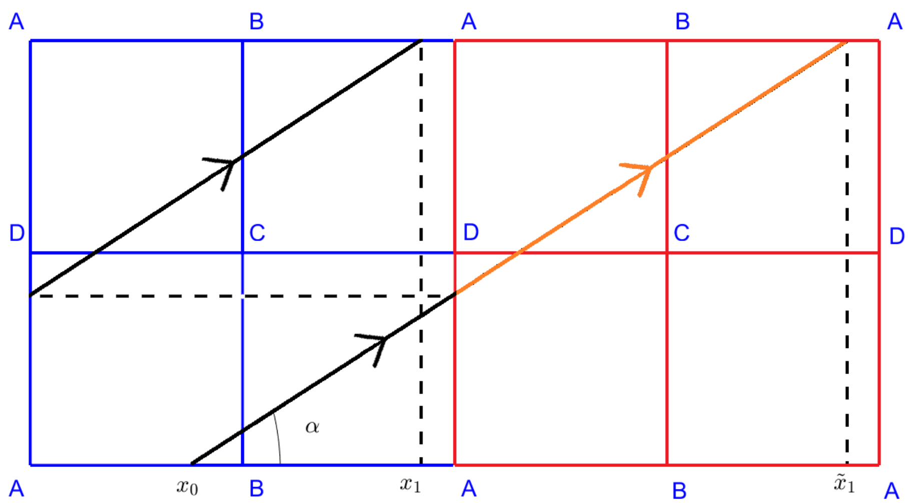

Figure A.1: Trajectory within $\mathbb{K}_2$ in blue and within $\mathbb{R}^2$ (one horizontal translation).

triangle with height 2 and base $\tilde{x}_1 - x_0$ gives $\tan(\alpha) = \frac{2}{\tilde{x}_1 - x_0}$. Combining this with the result $\tilde{x}_1 = x_1 \pmod 2$ yields $x_1 = x_0 + 2\cot\alpha \pmod 2$. □

Observe that the square return map is a circle/rotation map with rotation number $2\cot(\alpha)$. A periodic orbit in the return map corresponds to a trajectory revisiting the base in the same location, as long as the revisiting angle is also the same (which must be the case by Proposition 2.11) . By inspection, a periodic orbit of the return map exists if and only if the rotation number is rational.

It may be tempting to simplify the return map to the form: $x_{n+1} = x_n + \cot(\alpha) \pmod 1$ as done in [34]. However, this removes useful information as x_n does not describe the revisited position for a trajectory within the square. From Figure A.1, the square in the bottom right has reversed horizontal orientation. When we revisit the base in this square, the true position of the trajectory will be $1 - x$ due to the orientation. Denote $\tilde{P}_n$ as the position on the base where the trajectory visits, it is described by:

$$\tilde{P}_{n+1} = \begin{cases} \tilde{P}_n + 2\cot(\alpha) \pmod 2, & \text{if } 0 \leq \tilde{P}_n + 2\cot(\alpha) \pmod 2 \leq 1, \\ 2 - [\tilde{P}_n + 2\cot(\alpha)] \pmod 2, & \text{if } 1 \leq \tilde{P}_n + 2\cot(\alpha) \pmod 2 \leq 2. \end{cases}$$

We now show this explicitly for a period-6 trajectory with $\alpha = \text{atan}(2)$; the argument for higher periodic orbits is more involved due to the increased number of different combinations of side collisions.

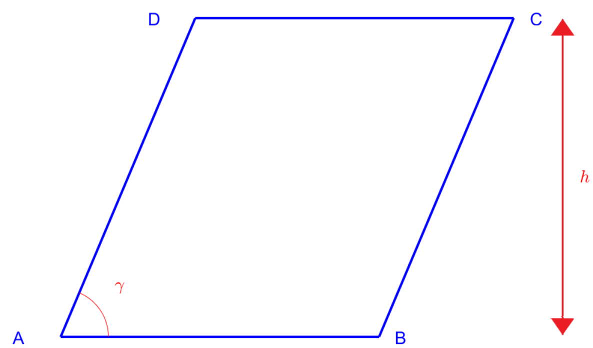

Figure A.2: The general parallelogram with height h and bottom left angle γ.

If $\alpha_0 = \text{atan}(2)$, then we have:

$$\tilde{P}_{n+1} = \begin{cases} (\tilde{P}_n + 1), \ (\text{mod}\, 2) & \text{if } 0 \leq (\tilde{P}_n + 1) \ (\text{mod}\, 2) \leq 1, \\ (1 - \tilde{P}_n), \ (\text{mod}\, 2) & \text{if } 1 \leq (\tilde{P}_n + 1) \ (\text{mod}\, 2) \leq 2. \end{cases}$$

Consider the trajectory with $P_0 = \tilde{P}_0 \in [0, 1]$. Then,

$$\begin{aligned} \tilde{P}_1 &= (\widetilde{P}_0 + 1)(\text{mod}\, 2) \in [1, 2] \\ &= (1 - \tilde{P}_0)(\text{mod}\, 2) \\ &= 1 - \tilde{P}_0 \in [0, 1] \end{aligned}$$

Using mathematical induction we can show that $\tilde{P}_{n+1} = 1 - \tilde{P}_n \in [0, 1]$. The return map has a fixed point at $\tilde{P} = 0.5$ and a derivative of -1 which implies a period-doubling bifurcation. We cannot apply the genericity conditions as our map is piecewise smooth and continuous; see Section 4.2.3.

A.3 The parallelogram map

Consider the parallelogram with height h and bottom left angle γ as depicted in Figure A.2. Due to symmetry, it is sufficient to consider $\gamma \in (0, \frac{\pi}{2}]$ and $h > 0$.

We map each of the four sides onto the interval $[0,\ 2 + \frac{2h}{\sin\gamma})$. The sub-interval $[0,\ 1)$ represents side 0, and the subsequent intervals $[1, 1 + \frac{h}{\sin\gamma})$, $[1 + \frac{h}{\sin\gamma}, 2 + \frac{h}{\sin\gamma})$ and $[2 + \frac{h}{\sin\gamma}, 2 + \frac{2h}{\sin\gamma})$ represent sides 1, $1 + \frac{h}{\sin\gamma}$ and $2 + \frac{h}{\sin\gamma}$, respectively. Let $P \in [0, 2(1 + \frac{h}{\sin\gamma})$ be the position at which the billiard collides with the boundary. Given the position, we note the side at which the collision occurs by $\underset{\sim}{\lfloor P \rfloor}$ where $\underset{\sim}{\lfloor \cdot \rfloor}$ is a modified floor function. We also define a modified ceiling function in the following:

Definition A.4. Let S be the set $\{0, 1, 1+\frac{h}{\sin\gamma}, 2+\frac{h}{\sin\gamma}\}$, then $\underset{\sim}{\lfloor\,\rfloor}, \underset{\sim}{\lceil\,\rceil} : [0, 2(1+\frac{h}{\sin\gamma})) \mapsto S$ are the functions $\underset{\sim}{\lfloor x \rfloor} = \max\{m \in S |\, m \leq x\}$ and $\underset{\sim}{\lceil x \rceil} = \min\{m \in S |\, m \geq x\}$.

We now define $\alpha \in (0, \pi)$ as the angle between the trajectory after collision and the line segment $(P, \underset{\sim}{\lceil P \rceil})$ (anti-clockwise angle with respect to the side). For brevity, let $x_n = P_n - \underset{\sim}{\lfloor P_n \rfloor}$. Given initial point (α_n, P_n), what is the next side that the trajectory collides with?

If $\underset{\sim}{\lfloor P_n \rfloor} \in \{0, 1+\frac{h}{\sin\gamma}\}$, i.e., the bottom or top side, then

$$\underset{\sim}{\lfloor P_{n+1} \rfloor} = \begin{cases} \underset{\sim}{\lfloor P_n \rfloor} + 1 \pmod{2+\frac{2h}{\sin\gamma}}, & \text{if } \alpha_n \in \left(0,\ \text{atan}\left(\frac{h}{1-x_n+h\cot\gamma}\right)\right), \\ \underset{\sim}{\lfloor P_n \rfloor} + 1 + \frac{h}{\sin\gamma} \pmod{2+\frac{2h}{\sin\gamma}}, & \text{if } \alpha_n \in \left(\text{atan}\left(\frac{h}{1-x_n+h\cot\gamma}\right),\ \text{atan}\left(\frac{h}{h\cot\gamma - x_n}\right)\right), \\ \underset{\sim}{\lfloor P_n \rfloor} + 2 + \frac{h}{\sin\gamma} \pmod{2+\frac{2h}{\sin\gamma}}, & \text{if } \alpha_n \in \left(\text{atan}\left(\frac{h}{h\cot\gamma - x_n}\right),\ \pi\right). \end{cases}$$

If $\underset{\sim}{\lfloor P_n \rfloor} \in \{1, 2+\frac{h}{\sin\gamma}\}$, i.e., the left or right side, then

$$\underset{\sim}{\lfloor P_{n+1} \rfloor} = \begin{cases} \underset{\sim}{\lfloor P_n \rfloor} + \frac{h}{\sin\gamma} \pmod{2+\frac{2h}{\sin\gamma}}, & \text{if } \alpha_n \in (0,\ \alpha_m), \\ \underset{\sim}{\lfloor P_n \rfloor} + 1 + \frac{h}{\sin\gamma} \pmod{2+\frac{2h}{\sin\gamma}}, & \text{if } \alpha_n \in (\alpha_m,\ \alpha'_m), \\ \underset{\sim}{\lfloor P_n \rfloor} + 1 + \frac{2h}{\sin\gamma} \pmod{2+\frac{2h}{\sin\gamma}}, & \text{if } \alpha_n \in (\alpha'_m,\ \pi), \end{cases}$$

where α_m satisfies $\frac{\sin(\gamma+\alpha_m)}{\sin\alpha_m} = \frac{h}{\sin\gamma} - x_n$ and α'_m satisfies $\frac{\sin(\gamma+\alpha'_m)}{\sin\alpha'_m} = -x_n$. By using a symbolic calculator, we can find explicit forms for α_m and α'_m. If $\frac{\sin(\gamma+\alpha)}{\sin\alpha} = y$, then $\alpha = \left(2\text{atan}\left(\frac{1}{2}\cot(\frac{\gamma}{2})(-y\tan^2\left(\frac{\gamma}{2}\right) + \sqrt{(\tan^2\left(\frac{\gamma}{2}\right)(y+1) + y - 1)^2 + 4\tan^2\left(\frac{\gamma}{2}\right)} - \tan^2\left(\frac{\gamma}{2}\right) - y + 1\right)\right) \pmod{4}$.

The new angle and position depend on which side we collide we with. If $\underset{\sim}{\lfloor P_n \rfloor} \in \{0, 1+\frac{h}{\sin\gamma}\}$. i.e., the bottom or top side, then

$$P_{n+1} = \underset{\sim}{\lfloor P_{n+1} \rfloor} + \begin{cases} \frac{\sin\alpha_n}{\sin(\gamma-\alpha_n)}(1-x_n), & \text{if } \underset{\sim}{\lfloor P_{n+1} \rfloor} = \underset{\sim}{\lfloor P_n \rfloor} + 1 \pmod{2+\frac{2h}{\sin\gamma}}, \\ 1 - x_n + h(\cot\gamma - \cot\alpha_n), & \text{if } \underset{\sim}{\lfloor P_{n+1} \rfloor} = \underset{\sim}{\lfloor P_n \rfloor} + 1 + \frac{h}{\sin\gamma} \pmod{2+\frac{2h}{\sin\gamma}}, \\ \frac{\sin\alpha_n}{\sin(\gamma-\alpha_n)}x_n + \frac{h}{\sin\gamma}, & \text{if } \underset{\sim}{\lfloor P_{n+1} \rfloor} = \underset{\sim}{\lfloor P_n \rfloor} + 2 + \frac{h}{\sin\gamma} \pmod{2+\frac{2h}{\sin\gamma}}, \end{cases}$$

and

$$\alpha_{n+1} = \begin{cases} \gamma - \alpha_n, & \text{if } \lfloor \underset{\sim}{P_{n+1}} \rfloor = \lfloor \underset{\sim}{P_n} \rfloor + 1 \left(\bmod 2 + \frac{2h}{\sin\gamma}\right), \\ \pi - \alpha_n, & \text{if } \lfloor \underset{\sim}{P_{n+1}} \rfloor = \lfloor \underset{\sim}{P_n} \rfloor + 1 + \frac{h}{\sin\gamma} \left(\bmod 2 + \frac{2h}{\sin\gamma}\right), \\ \pi - \alpha_n + \gamma, & \text{if } \lfloor \underset{\sim}{P_{n+1}} \rfloor = \lfloor \underset{\sim}{P_n} \rfloor + 2 + \frac{h}{\sin\gamma} \left(\bmod 2 + \frac{2h}{\sin\gamma}\right). \end{cases}$$

If $\lfloor \underset{\sim}{P_n} \rfloor \in \{1, 2 + \frac{h}{\sin\gamma}\}$, i.e., the left or right side, then

$$P_{n+1} = \lfloor \underset{\sim}{P_{n+1}} \rfloor + \begin{cases} \frac{\sin\alpha_n}{\sin(\gamma+\alpha_n)} \left(\frac{h}{\sin\gamma} - x_n\right), & \text{if } \lfloor \underset{\sim}{P_{n+1}} \rfloor = \lfloor \underset{\sim}{P_n} \rfloor + \frac{h}{\sin\gamma} \left(\bmod 2 + \frac{2h}{\sin\gamma}\right), \\ \frac{h}{\sin\gamma} - \frac{\sin(\gamma+\alpha_n)}{\sin\alpha_n} - x_n, & \text{if } \lfloor \underset{\sim}{P_{n+1}} \rfloor = \lfloor \underset{\sim}{P_n} \rfloor + 1 + \frac{h}{\sin\gamma} \left(\bmod 2 + \frac{2h}{\sin\gamma}\right), \\ 1 + \frac{\sin\alpha_n}{\sin(\gamma+\alpha_n)} x_n, & \text{if } \lfloor \underset{\sim}{P_{n+1}} \rfloor = \lfloor \underset{\sim}{P_n} \rfloor + 1 + \frac{2h}{\sin\gamma} \left(\bmod 2 + \frac{2h}{\sin\gamma}\right), \end{cases}$$

and

$$\alpha_{n+1} = \begin{cases} \pi - \gamma - \alpha_n, & \text{if } \lfloor \underset{\sim}{P_{n+1}} \rfloor = \lfloor \underset{\sim}{P_n} \rfloor + \frac{h}{\sin\gamma} \left(\bmod 2 + \frac{2h}{\sin\gamma}\right), \\ \pi - \alpha_n, & \text{if } \lfloor \underset{\sim}{P_{n+1}} \rfloor = \lfloor \underset{\sim}{P_n} \rfloor + 1 + \frac{h}{\sin\gamma} \left(\bmod 2 + \frac{2h}{\sin\gamma}\right), \\ 2\pi - \alpha_n - \gamma, & \text{if } \lfloor \underset{\sim}{P_{n+1}} \rfloor = \lfloor \underset{\sim}{P_n} \rfloor + 1 + \frac{2h}{\sin\gamma} \left(\bmod 2 + \frac{2h}{\sin\gamma}\right). \end{cases}$$

Lemma A.5. *The boundary values α_m and α'_m of for our parallelogram map reside in the intervals $(0, \pi - \gamma)$ and $(\pi - \gamma, \pi)$ respectively.*

Proof. By definition, α'_m satisfies $\frac{\sin(\gamma+\alpha'_m)}{\sin\alpha'_m} = -x_n$ with $\gamma \in (0, \frac{\pi}{2})$ and $\alpha'_m \in (0, \pi)$. The right-hand side is negative and in order for the left-hand side to be also negative, the numerator and denominator must be of opposite signs. We plot the numerator and denominator in Figure A.3; observe that this occurs for $\alpha'_m \in (\pi - \gamma, \pi)$. The same argument applies for α_m with a positive right-hand side. ☐

A.3.1 Period-2 orbits within the parallelogram

It is natural to visualise a period-2 orbit that exists with $\alpha_0 = \frac{\pi}{2}$ that collides with the top and bottom horizontal sides. However, as a corollary to the derivation, we have a proof that there always exists also a period-2 orbit in the square when starting from the angled sides with an angle of $\frac{\pi}{2}$. We find that setting $\alpha_0 = \frac{\pi}{2}$ for any $P \in (h\cot(\gamma),\ 1)$ on side 0 or any $P \in \left(1 + \frac{h}{\sin\gamma} + h\cot\gamma,\ 2 + \frac{h}{\sin\gamma}\right)$ on side $1+\frac{h}{\sin\gamma}$ will exhibit a period-2 orbit; see Figure A.4. There does not exist any period-2 orbits between the base/top sides and the angled right/left

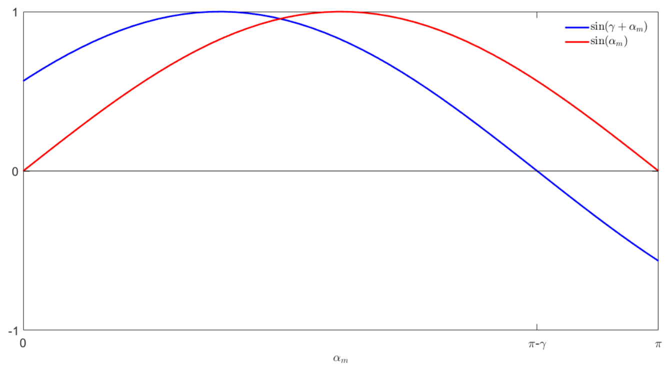

Figure A.3: Plot of α_m against $\sin(\alpha_m)$ and $\sin(\gamma + \alpha_m)$ in red and blue, respectively.

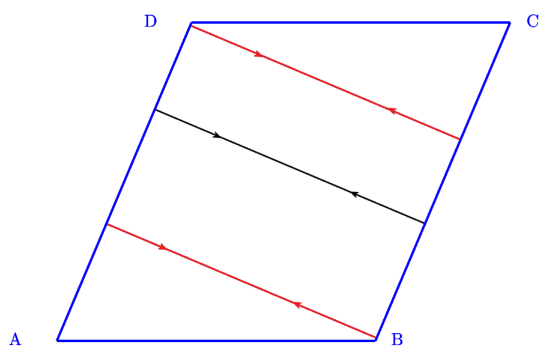

Figure A.4: Period-2 trajectories between the angled sides of a parallelogram. The red trajectories are give the minimum and maximum positions that collide with the opposite side.

sides as the return angle would not match α_0. For $\gamma \in (0, \text{atan}(h))$, the base and top of the parallelogram will not overlap. Therefore, for these γ, we cannot have any period-2 orbits between the base and top. However, as a corollary to our parallelogram billiard map, we find that period-2 orbits between the angled left/right sides exist for all parallelograms.

Corollary A.6. *There always exists a period-2 orbit within the parallelogram billiard.*

A.3.2 Period-3 orbits within the parallelogram

As with the square and rectangle, the parallelogram does not exhibit any period-3 orbits. We use our geometric proof for the non-existence proof for period-3 orbits within the square in Proposition 2.5 as inspiration. Note that we still must collide with three unique sides, the only difference in argument is that we now have to account for two different cases: starting from the base or on the angled side.

Proposition A.7. *There do not exist any period-3 orbits within the parallelogram billiard.*

A.3.3 Parallelogram area function

The area of a periodic orbit for the parallelogram is defined analogously to the square/rectangle special case given in Section 3.4.1. We are interested in the outside triangle areas when visiting the adjacent sides.

Definition A.8. A period-T orbit that visits positions $\{P_0, \ldots, P_{T-1}\}$, has area $A = T - \sum_{i=0}^{T-1} \tilde{a}_i$, where $x_i = P_i - \lfloor \underset{\sim}{P_i} \rfloor$,

if $\lfloor \underset{\sim}{P_i} \rfloor \in \{0, 1 + \frac{h}{\sin\gamma}\}$,

$$\tilde{a}_i = \begin{cases} \frac{1}{2}(1 - x_i)x_{i+1}\sin(\gamma), & \text{if } \lfloor \underset{\sim}{P_{i+1}} \rfloor = \lfloor \underset{\sim}{P_i} \rfloor + 1 \pmod{2 + \frac{2h}{\sin\gamma}}, \\ 0, & \text{if } \lfloor \underset{\sim}{P_{i+1}} \rfloor = \lfloor \underset{\sim}{P_i} \rfloor + 1 + \frac{h}{\sin\gamma} \pmod{2 + \frac{2h}{\sin\gamma}}, \\ \frac{1}{2}x_i(h - x_{i+1})\sin(\gamma), & \text{if } \lfloor \underset{\sim}{P_{i+1}} \rfloor = \lfloor \underset{\sim}{P_i} \rfloor + 2 + \frac{h}{\sin\gamma} \pmod{2 + \frac{2h}{\sin\gamma}}, \end{cases}$$

and if $\lfloor \underset{\sim}{P_i} \rfloor \in \{1, 2 + \frac{h}{\sin\gamma}\}$,

$$\tilde{a}_i = \begin{cases} \frac{1}{2}(h - x_i\sin(\gamma))x_{i+1}, & \text{if } \lfloor \underset{\sim}{P_{i+1}} \rfloor = \lfloor \underset{\sim}{P_i} \rfloor + \frac{h}{\sin\gamma} \pmod{2 + \frac{2h}{\sin\gamma}}, \\ 0, & \text{if } \lfloor \underset{\sim}{P_{i+1}} \rfloor = \lfloor \underset{\sim}{P_i} \rfloor + 1 + \frac{h}{\sin\gamma} \pmod{2 + \frac{2h}{\sin\gamma}}, \\ \frac{1}{2}x_i(1 - x_{i+1})\sin(\gamma), & \text{if } \lfloor \underset{\sim}{P_{i+1}} \rfloor = \lfloor \underset{\sim}{P_i} \rfloor + 1 + \frac{2h}{\sin\gamma} \pmod{2 + \frac{2h}{\sin\gamma}}. \end{cases}$$

A.3.4 Numerical settings and results

When calculating the Jacobian for Newton's method, we use central difference method for all the derivatives with $h = 10^{-6}$.

$$\frac{\partial f}{\partial \alpha} \approx \frac{f(\alpha + h, P) - f(\alpha - h, P)}{2h}$$

For periodic orbits, we need a higher order map, we remedy this by simply adding superscripts to all:

$$\frac{\partial f^{(N)}}{\partial \alpha} \approx \frac{f^{(N)}(\alpha + h, P) - f^{(N)}(\alpha - h, P)}{2h}.$$

Denote A as our area function, the mixed partials also use central difference method except at the end points which use forward and backward.

$$\frac{\partial^2 A}{\partial P^2} \approx \frac{A(\alpha, P + h) - 2A(\alpha, P) + A(\alpha, P - h)}{h^2}$$

$$\frac{\partial^2 A}{\partial\alpha\partial P} \approx \frac{A(\alpha+h,P+h)-A(\alpha+h,P-h)-A(\alpha-h,P+h)+A(\alpha-h,P-h)}{4h^2}$$

Parameter continuation only terminates if both the ℓ_2 norm of the successive differences is below 10^{-6}, the absolute value of each component in $F(\alpha, P)$ is below 10^{-8} and if the additional constraint: $f^{(N)}(\alpha, P) - \alpha = 0$ is satisfied to within 10^{-6}.

For the continuation of the periodic orbits which exhibit the period-adding bifurcation in Section 4.2.3, we show some of the numerical results in Figure A.5. Panel (a) shows the number of Newton steps is 0 for large γ, this is when we follow the period-2 orbits as all period-2 orbits maximise area, we do not need to perform any Newton iterations. All the other step counts are either 2 or 3 which implies that parameter continuation is behaving appropriately (i.e., we have not jumped onto a different solution branch). Panel (b) shows the area of each periodic orbit, the jumps here indicate when a period-adding bifurcation has occurred. Observe that as γ decreases (or as the period increases), the area decreases in a cascading manner. Note that the area plot has been appropriately scaled as we are effectively following a period-1748648318376960000 orbit. Figure A.6 is a companion figure to 4.6 which is analogous to the left and right panels of Figure 4.4. We vary P_0 for a fixed $\alpha_0 = \frac{\pi}{2}$ which is determined by parameter continuation and plot it on horizontal axis. On the vertical axis we have P_N, where $N = 2, 6, 10$ and 14 for panels (a)-(b), (c)-(d), (e)-(f), (g)-(h), respectively. Period-N orbits lie on the blue line $P_0 = P_N$, the red segments display the actual map value $g(\alpha_0; P_0)$. Therefore if a red point lies on $P_0 = P_N$, it may potentially be a period-N orbit. For each panel in alphabetical order, the γ is: $\frac{\pi}{2}$, 0.8298, 0.7297, 0.5760, 0.5659, 0.4888, 0.4887 and 0.4488, respectively. Observe that as γ decreases the measure of positions which support a period orbit also decrease but do not tend to zero as in Section 4.2.2 and in Figure 4.4. This is potentially a reason for why we are able to follow these solutions through vertices but are unable to for the solutions in Section 4.2.2.

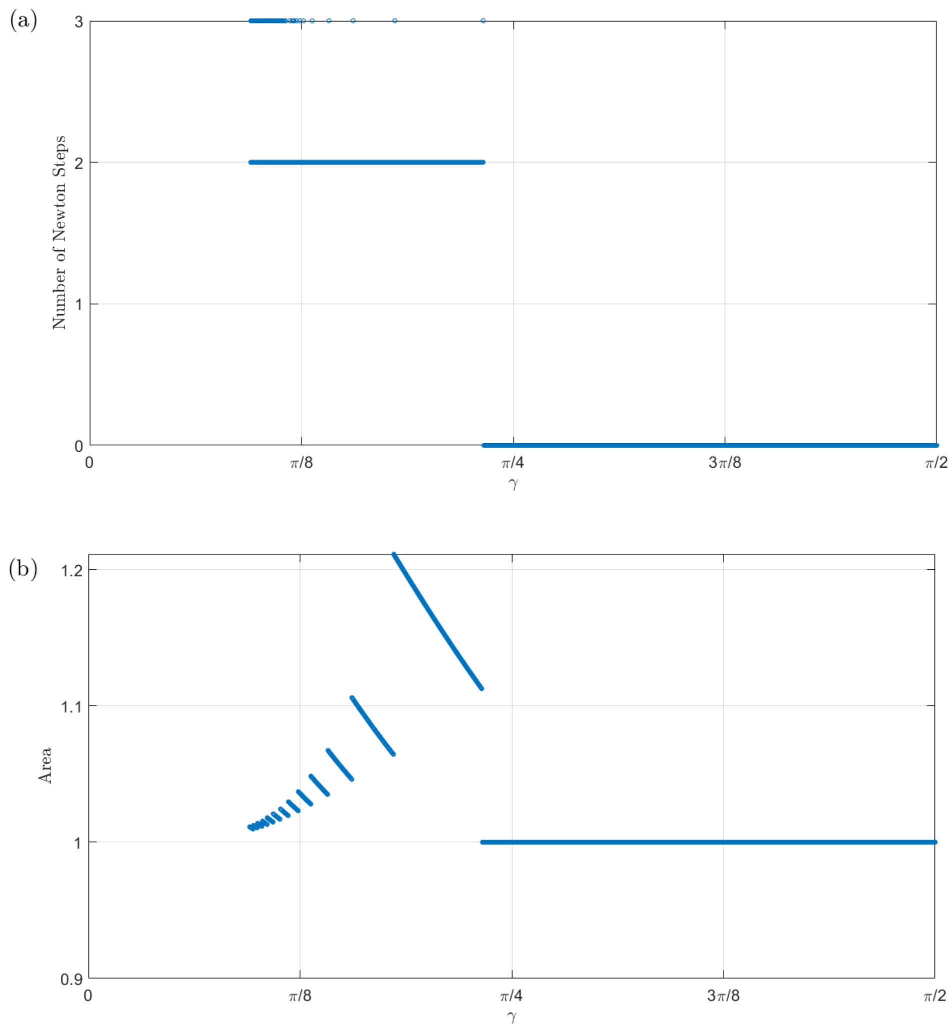

Figure A.5: Numerical results for the period-adding parameter continuation. Panel (a) and panel (b) show the number of Newton steps and the area as we follow solutions in γ, respectively.

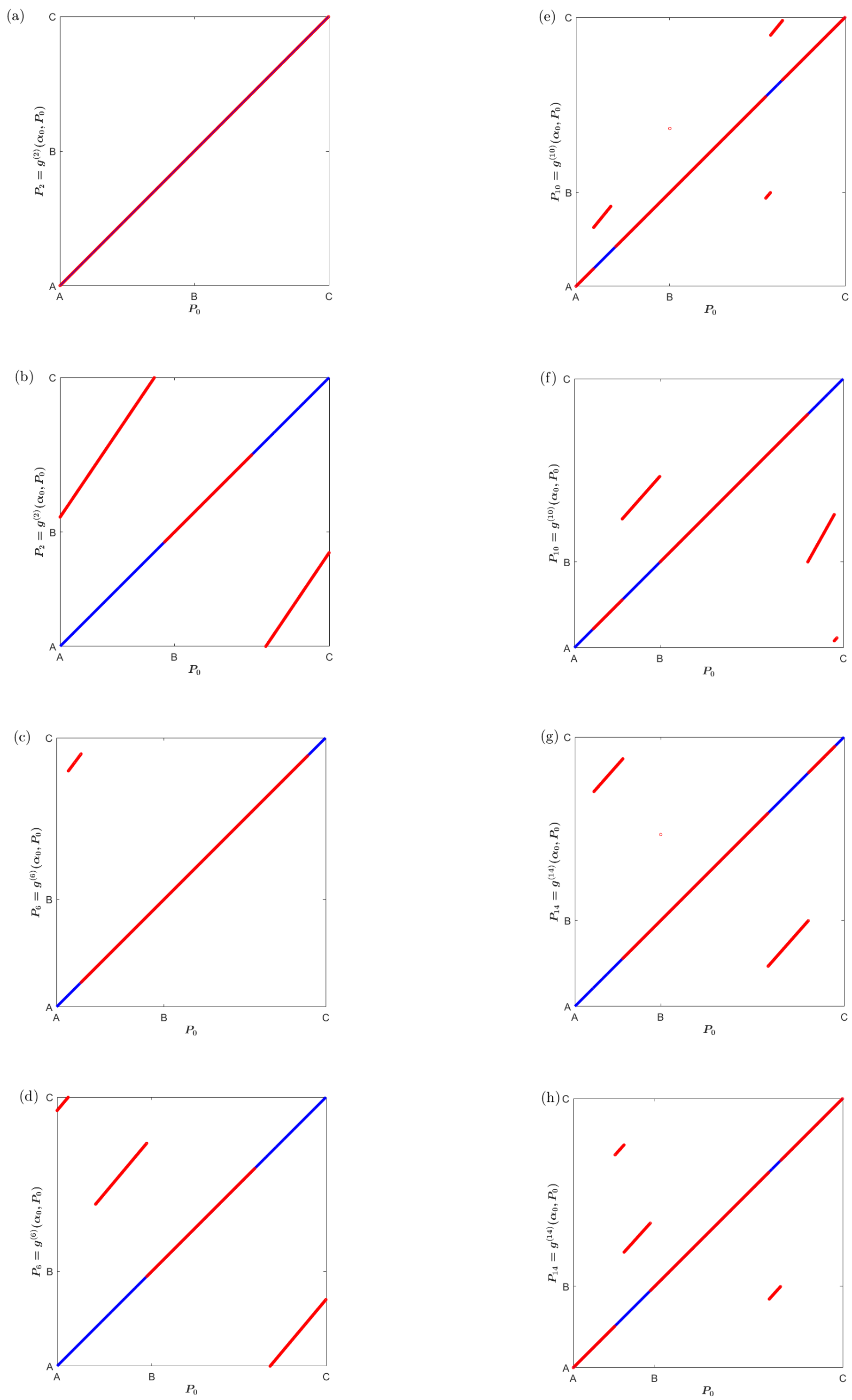

Figure A.6: Panels (a)-(b), (c)-(d), (e)-(f), (g)-(h) each depict the 2nd, 6th, 10th and 14th iterate of the position map g for varying P_0 with fixed α_0 determined by the convergence of parameter continuation. For each panel in alphabetical order, γ is: $\frac{\pi}{2}$, 0.8298, 0.7297, 0.5760, 0.5659, 0.4888, 0.4887 and 0.4488, respectively. This is a companion figure to Figure 4.6.